International Journal of Solids and Structures 309 (2025) 113196

Contents lists available at ScienceDirect

International Journal of Solids and Structures

journal homepage: www.elsevier.com/locate/ijsolstr

Rate dependent self-healing model for cementitious materials

Sina Sayadi *, Iulia Mihai, Anthony Jefferson

School of Engineering, Cardiff University, Queen's Buildings, The Parade, Cardiff, CF24 3AA Wales, United Kingdom

ARTICLE INFO

Keywords:
Micromechanical model
Rate-dependent healing
Finite element analysis
Self-healing

ABSTRACT

A new micromechanics-based constitutive model for self-healing cementitious materials is proposed. The model is aimed at self-healing materials with distributed healing mechanisms, such as materials with embedded microcapsules and enhanced autogenous healing capabilities. The model considers anisotropic microcracking and time-dependent healing. In contrast to many existing models for self-healing cementitious materials, the new approach imposes no limitations on the number or timing of microcracking or healing events that can be simulated. The formulation ensures that the simulation of microcracking and healing is always consistent with the second law of thermodynamics. The model is implemented in a three-dimensional nonlinear finite element code that allows structural elements formed from self-healing materials to be simulated. A series of single-point simulations illustrate the versatility of the model. The experiments considered with the model encompass a set of cylindrical specimens formed from concrete with embedded microcapsules containing sodium silicate, and a notched beam test series that examined the self-healing potential of concrete formed with a crystalline admixture. The validations show that the model can capture the characteristic mechanical behaviour of these structural elements with good engineering accuracy.

1. Introduction

There has been strong interest in the development of self-healing cementitious materials (SHCM) over the last two decades due to the need to improve the durability and resilience of civil engineering structures. The development, design and assessment of these SHCM structures requires accurate and robust models that can capture their fundamental behaviour, particularly in the absence of design codes of practice. The earliest models for self-healing systems simulated wound healing. These models (Arnold and Adam, 1999; van Vermolen et al., 2006) considered a diffusion process to capture healing growth within designated wound layers. Although the development of biomimetic construction materials is inspired by natural processes in biological systems, the underlying cracking and healing mechanisms differ significantly from those of their organic counterparts. Self-healing in cementitious materials involves a series of physical and chemical processes (Shields et al. 2021; Van Tittelboom & De Belie 2013) that include: i) mechanical cracking and healing, ii) fluid and heat transport, and iii) chemical reactions and the associated curing of healing agents.

Various approaches have been explored to capture the behaviour of SCHMs in cracking-healing cycles, and several coupled models have been presented that can simulate these processes (Jefferson *et al.* 2018). In recent studies, morphological methods have been employed to establish a mathematical relationship between healing mechanisms and post-healed mechanical properties (Lee & Anthony 2023; Ponnusami et al. 2019; Zhou et al. 2017). However, most existing models are either fully or semi-empirical in nature and require considerable experimental data to calibrate their response for a particular SCHM. This implies that these models are only valid within the data range considered.

In general, two general approaches have been employed to simulate mechanical self-healing processes; namely, the discrete crack approach (Abu Al-Rub 2016; Cibelli et al. 2022; Freeman *et al.* 2020; Jefferson & Freeman 2022) and the smeared crack approach (Davies & Jefferson 2017; Dutta & Kishen 2019; Han et al. 2021a; James et al. 2014; Zhou et al. 2016; Zhu et al. 2015, 2016).

Several constitutive models have employed Continuum Damage Healing Mechanics (CDHM) as a modelling framework (Oucif & Mauludin 2018). In this approach, the evolution of healing is linked to the degree of damage by introducing a healing variable (scalar or tensor) that describes the proportion of the effective damage area that has healed. This progresses according to a phenomenological healing evolution function (Abu Al-Rub & Darabi 2012; Darabi et al. 2012).

For ductile materials, the elastoplastic constitutive formulation proposed by Barbero et al. (2005) has been used by several authors

* Corresponding author.
E-mail address: Sayadimoghadams@cardiff.ac.uk (S. Sayadi).

https://doi.org/10.1016/j.ijsolstr.2024.113196
Received 24 January 2024; Received in revised form 9 December 2024; Accepted 10 December 2024
Available online 14 December 2024

(Voyiadjis et al. 2011). This formulation uses the concept of elastic strain energy equivalence to derive damage-healing tensors. This idea was subsequently extended by Subramanian & Mulay (2022) to encompass self-healing in shape memory polymers.

Several investigators have shown that micromechanics-based models are able to describe the behavioural characteristics of multiphase quasi-brittle materials (Monchiet et al. 2012). In the case of cementitious materials, a micromechanical formulation has been employed to represent various mechanisms and processes, including the hydration reactions of distinct phases within a cement paste (Königsberger et al. 2020; Pichler et al. 2013; Pichler & Hellmich 2011). The micromechanics approach has also been used to simulate the effects of microcracks on the overall response of cement paste arising from early-age cracking and/or mechanical loading (Dutta & Kishen 2019; Pensée et al. 2002; Pichler et al. 2007).

Employing micromechanics formulations to represent cracking in quasi-brittle composite materials has also enabled the development of mechanistic models suitable for self-healing applications in these materials. Chen et al. 2022; Zhu & Arson 2014; Zhu et al. 2015, 2016 employed a 2D micromechanical framework to simulate the behaviour of microencapsulation self-healing systems under tensile and compressive loads. They used classical fracture mechanics to establish a microcracking evolution relationship and derived a compliance tensor for the healed material. Subsequently, Chen et al. (2022) considered aligned penny-shaped microcracks to evaluate the overall compliance matrix for concrete after healing as a function of the crack healing ratio. In their formulation, crystallization reaction kinetics was used to compute the degree of healing.

In another significant study, Davies and Jefferson (2017) developed a 3D model aimed at describing autogenous self-healing in cementitious materials. The model is able to simulate anisotropic microcracking and healing, but healing was considered to be instantaneous and thus the model did not consider the time-dependent nature of healing. The majority of these models considered single healing events although some also incorporated re-damage in their mathematical formulations (Oucif & Mauludin 2018).

More recently, Han et al. 2021a, 2021b proposed a micromechanical formulation to simulate the mechanical behaviour of self-healing concrete. Their approach adopted linear fracture mechanics criteria for both damage initiation and evolution. In a broader context, Sanz-Herrera et al. (2019) introduced a comprehensive framework that considers multiple healing cycles in self-healing materials, based on the assumption that each healing step is initiated under fully unloaded conditions.

In this paper, a micromechanics-based constitutive model for SHCMs is presented, which incorporates directional microcracking and rate-dependent healing. The primary novel aspect of the work is the introduction of rate dependent healing into a micromechanical model that does not have restrictions on the number of healing cycles, the strain conditions under which healing takes place, and which also allows simultaneous microcracking and healing. This builds on previous work by the authors' team on micromechanical models for cementitious composites (Mihai and Jefferson, 2011) and −specifically- on the work of Davies and Jefferson (2017) on a micromechanical model for self-healing cementitious materials, which had considerable restrictions, as explained above. This research also draws upon the theory developed for a discrete damage-healing model that was applied to elements with embedded strong discontinuities (Jefferson and Freeman, 2023). A second, more arcane, contribution relates to the strict enforcement of the condition that there should be zero-stress change during an increment of pure healing. This condition is important for ensuring that spurious energy is not created during healing. The way that this condition was considered in Davies and Jefferson's model is inadequate for the more general microcracking-healing scenarios of this paper.

The layout of the remainder of this paper is as follows; section 2 presents the basic model theory followed by a description of its numerical implementation; in section 3 the constitutive response predicted by the model is illustrated using a series of single material point simulations, and this is followed by the presentation of a boundary value problem in section 4. Finally, the main conclusions from the work are drawn in section 5. In this paper, the only damage considered is mechanical loss of strength and stiffness due to microcracking.

2. Constitutive formulation for microcracking and healing

The main concepts of the constitutive model are presented in Fig. 1. The cementitious composite is modelled as an elastic solid containing a series of randomly distributed circular microcracks which can have any orientation, defined by ψ and θ (see Fig. 1a). Each direction has a set of local unit vectors, with the vector $\mathbf{r}$ being normal to the microcrack plane, and $\mathbf{s}$ and $\mathbf{t}$ being in-plane vectors. The model simulates healing using time dependent variables to describe the repair of these directional microcracks (see Fig. 1b). In addition, a set of healing strain tensors are introduced for every local microcracking direction to simulate the permanent strains that occur when healing agent cures in open microcracks. The formulation ensures that no spurious energy is created when healing occurs.

2.1. Constitutive equations for a model with directional microcracking

The model draws on a series of previous micromechanics-based constitutive formulations for cementitious materials (Davies & Jefferson, 2017; Jefferson & Bennett 2007; Jefferson and Bennett, 2010; Mihai & Jefferson 2011). The essential equations from the underlying micromechanical model, required for the derivation of the new healing model, are summarised in Table 1. In the Table, 'total' refers stress, strain and constitutive tensors in Cartesian axes, and 'local' refers to directional terms, which are either integrated to give the total terms (see equation 2) or transformed from total tensors (see equations 8 and 9).

Fig. 2a illustrates the microcracking strain surface (equation 5) and Fig. 2b shows a set of parallel microcracks in the cementitious composite.

2.2. Derivation of model constitutive equations

Healing is simulated by the addition of a new term to the right-hand-side of the local constitutive equation (4) such that the local stress in an RME comprises two components, the first term representing the proportion of un-microcracked material, and the second term giving the proportion of healed – re-microcracked material. The resulting equation is as follows:

$$\mathbf{s}_{\mathrm{Lh}} = (1-\omega)\mathbf{D}_{\mathrm{L}}\colon \boldsymbol{\varepsilon}_{\mathrm{L}} + h_v(1-\omega_h)\mathbf{D}_{\mathrm{Lh}} : (\boldsymbol{\varepsilon}_{\mathrm{L}} - \boldsymbol{\varepsilon}_{\mathrm{h}}) \tag{10}$$

where $\mathbf{s}_{\mathrm{Lh}}$, which replaces $\mathbf{s}$ used in equation 4, is the local stress tensor allowing for any healing, and $\mathbf{D}_{\mathrm{Lh}}$ the local elasticity matrix of the healed material, $\boldsymbol{\varepsilon}_{\mathrm{h}}$ is the healing strain and ω_h is the re-microcracking variable. It is noted that $\mathbf{s}_{\mathrm{Lh}}, \omega, \boldsymbol{\varepsilon}_{\mathrm{L}}, \omega_h, \boldsymbol{\varepsilon}_{\mathrm{L}}$ & $\boldsymbol{\varepsilon}_{\mathrm{h}}$ all vary with time (t) and with direction (ψ and θ), but these dependencies have been omitted for clarity of presentation.

The healing variable ($h_v \in [0,\ \omega]$) represents the proportion of microcracked material that is healed at a given time in the absence of re-microcracking. More specifically, h_v is equal to the maximum healing front position, in increasing microcracking terms, in a given direction. The evolution of h_v for the present micromechanical model is explained in section 2.3. The model accounts for re-microcracking of healed material by employing a second microcracking variable ($\omega_h \in [0,1]$), which gives the proportion of h_v that has re-microcracked. When healed material re-microcracks, ω_h evolves according to equations (11) and (12), which are the healing counterparts to equations (7) and (5) respectively.

$$\omega_h(\zeta_h) = 1 - \frac{\varepsilon_t}{\zeta_h} e^{-c\left(\frac{\zeta_h - \varepsilon_{ht}}{\varepsilon_{h0} - \varepsilon_{ht}}\right)} \tag{11}$$

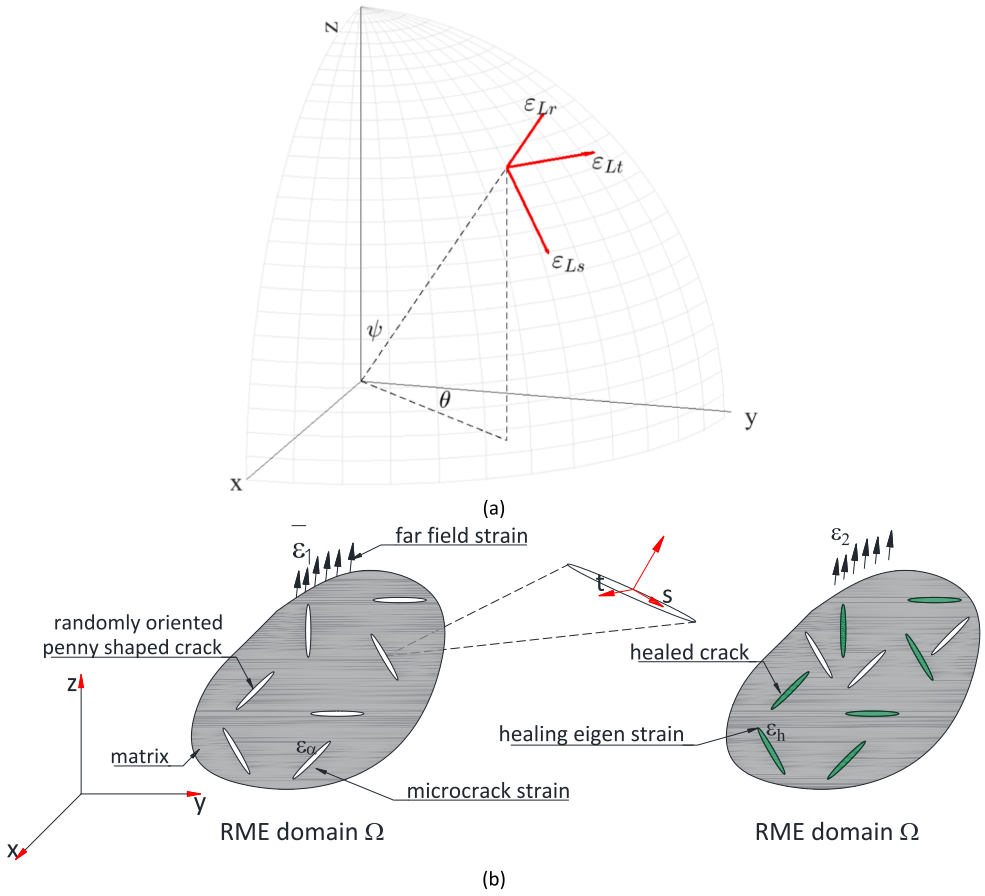

Fig. 1. Schematic representation of RME. a) Coordinate system: b) illustration of microcracked (left) and partially healed (right), material states.

Table 1
Summary of equations from the underlying microcracking model.

Equation	Number	Description (Jefferson and Bennett, 2007 & 2010)
$\sigma = \mathbf{D} : (\boldsymbol{\varepsilon} - \boldsymbol{\varepsilon}_{\text{add}})$	(1)	Total constitutive relationship.
$\boldsymbol{\varepsilon}_{\text{add}} = \frac{1}{2\pi}\iint_S \mathbf{N}_\varepsilon : \boldsymbol{\varepsilon}_\alpha \, \mathrm{dS}$	(2)	Total added strain tensor obtained by integrating the local added strain tensor (which varies with direction) over a hemisphere.
$\boldsymbol{\varepsilon}_\alpha = \left(\frac{\omega}{1-\omega}\right)\mathbf{C}_\text{L} : \mathbf{s}$	(3)	Local added strain tensor in terms of the local stress, elastic compliance and local microcracking variable.
$\mathbf{s} = (1-\omega)\mathbf{D}_\text{L} : \boldsymbol{\varepsilon}_\text{L}$	(4)	Local constitutive relationship in terms of the local strain (sum of elastic and added local strains) and local elasticity tensor.
$F_\zeta(\boldsymbol{\varepsilon}_L, \zeta) = \zeta_{ef}(\boldsymbol{\varepsilon}_L) - \zeta = 0$	(5)	Microcracking function in terms of the local microcracking strain (ζ_{ef}) (see footnotes) and the local microcracking strain parameter.
subject to $F_\zeta \le 0; \dot{\zeta} \ge 0; F_\zeta \dot{\zeta} = 0$	(6)	$F_\zeta(\boldsymbol{\varepsilon}_L, \zeta)$ is subject to the Karush–Kuhn–Tucker conditions, equation (6), which are applied to equation (5) such that local strains remain on the microcracking surface when local microcracking is active in a particular direction (Mihai & Jefferson, 2012). In the present case, this involves updating ζ to the value of $\zeta_{ef}(\boldsymbol{\varepsilon}_L)$, if the latter exceeds the value of the former from the last converged state.
$\omega(\zeta) = 1 - \frac{\varepsilon_t}{\zeta} e^{-c\left(\frac{\zeta-\varepsilon_t}{\varepsilon_0-\varepsilon_t}\right)}$	(7)	Local microcracking variable in terms of the microcracking strain parameter.
$\mathbf{s} = \mathbf{N} : \boldsymbol{\sigma}$	(8)	Transformations for local stress and strain from their total counterparts.
$\boldsymbol{\varepsilon}_\text{L} = \mathbf{N}_\varepsilon^{\text{T}} : \boldsymbol{\varepsilon}$	(9)	

Notation and notes.
$\boldsymbol{\varepsilon}_{\text{add}}$ is the overall additional strain tensor due to microcracking, $\boldsymbol{\sigma}$ and $\boldsymbol{\varepsilon}$ are the total stress and strain tensors respectively, $\mathbf{D}$ is the elasticity tensor, $\mathbf{N}$ is the stress transformation tensor, $\mathbf{N}'$, in matrix terms, is equal to $\mathbf{N}^\text{T}$, $\mathbf{N}_\varepsilon$ is a strain transformation tensor, $\boldsymbol{\varepsilon}_\alpha$ is the local added strain tensor, S denotes the surface of a unit hemisphere, ω is the directional microcracking variable, $\mathbf{C}_\text{L}$ is the local elastic compliance tensor, $\mathbf{s}$ is the local stress tensor, $\mathbf{D}_\text{L} = \mathbf{C}_\text{L}{}^{-1}$ is the local elasticity tensor, ε_L is a local strain tensor that comprises the sum of the added (ε_α) and the elastic ($\varepsilon_{\text{L}e}$) local strains, F_ζ is the microcracking function (also known as the local microcracking strain surface), ζ_{ef} is the effective microcracking strain (see below), ζ is the microcracking strain parameter, c is the microcrack evolution constant, $\varepsilon_0 = u_o/\ell_e$ is the strain at the fully microcracked state, u_o is displacement at the end of the softening curve, ℓ_e is the finite element characteristic length, $\varepsilon_t = f_t/E, f_t$ is the uniaxial tensile stress at which microcracking initiates and E is Young's modulus of the cementitious matrix material. Local tensors are expressed in a reduced vector or matrix form in which only those terms that can be non-zero are included e.g. $\mathbf{s} = [s_{rr} s_{rs} s_{rt}]^\text{T}$.

$\zeta_{ef}(\boldsymbol{\varepsilon}_\text{L}) = \left(\frac{\varepsilon_{Lrr}}{2}\left(1 + \left(\frac{\mu}{q}\right)^2\right) + \frac{1}{2q^2}\sqrt{\varepsilon_{Lrr}^2(q^2-\mu^2)^2 + 4q^2\gamma^2}\right)$, in which $\mu = \frac{\mu_s E}{G}$, $\gamma = \sqrt{\varepsilon_{Lrs}^2 + \varepsilon_{Lrt}^2}$, $q = \frac{q_s E}{G}$, μ_s is an internal friction parameter and q_s is the ratio of interface shear strength to matrix tensile strength.

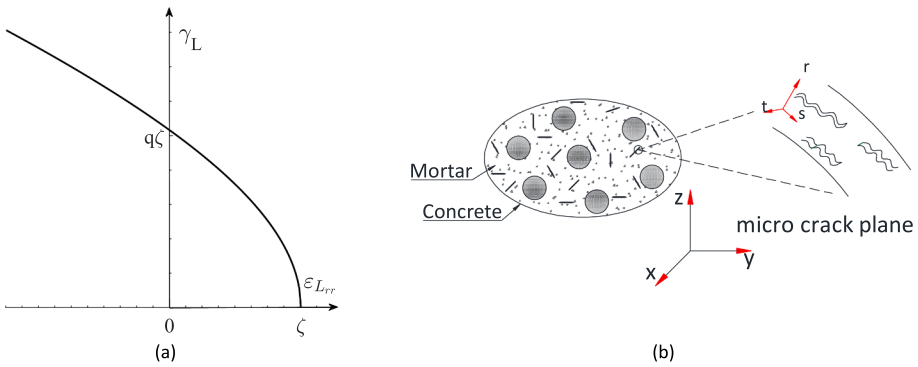

Fig. 2. Microcracking strain surface, b) parallel set of microcracks.

$$F_{\zeta h}(\boldsymbol{\varepsilon}_L, \boldsymbol{\varepsilon}_h, \zeta) = \zeta_{hef}(\boldsymbol{\varepsilon}_L - \boldsymbol{\varepsilon}_h) - \zeta_h = 0 \tag{12}$$

where $\zeta_{hef}, \zeta_h, \varepsilon_{h0}\&\varepsilon_{ht}$ are the healing counterparts to the microcracking function/parameters $\zeta_{ef}\zeta, \varepsilon_0\&\varepsilon_t$. It is noted that when re-healing occurs, ω_h reduces, as explained below.

The general form of equation (10) is similar to the local constitutive equation employed by Davies and Jefferson (2017), but the meaning of the healing and re-microcracking variables and the way that they are updated are quite different. This is because the model by Davies and Jefferson only allowed one healing and one re-microcracking event. Furthermore, in their model, healing terms did not evolve over time.

When healing agent cures in an open microcrack, there is a moment in time when solid material first bridges between the opposing crack faces. This is when mechanical healing of the crack commences, and it is assumed that this bridging material is stress free at the time of formation. This 'stress free at formation' condition is assumed to apply to every new increment of bridging material. This assumption is not only consistent with experimental data (Selvarjoo et al. 2020), but also ensures that the simulation of healing does not create spurious energy and therefore does not violate the second law of thermodynamics. Expanding on this issue; when healing is simulated, the stiffness of the material increases. Thus, if the strain remained constant, the stress and the strain energy would increase. This would violate the second law unless the increase in strain energy was matched by the release of thermal-chemical energy. Since there is no evidence that the stress rises during healing, the surest way to ensure that the model satisfies thermodynamics principles is to introduce a healing strain (ε_h) that evolves such that the stress does not change due to healing alone. Furthermore, this strain simulates the permanent strains associated with solidified healing agent, which prevents microcracks from fully closing. This permanent strain is evident in experiments in which healing has occurred in open cracks (Selvarajoo et al., 2020). A mathematical treatment of this issue may be found in Appendix B of Jefferson and Freeman (2022), in the context of a discrete cracking model. The method used to update $\boldsymbol{\varepsilon}_h$ is discussed below.

The derivation now proceeds by determining the total inelastic strain tensor for each direction, which is the equivalent of equation (3). This is accomplished by rearranging equation (10) to give the local strain, as follows:

$$\boldsymbol{\varepsilon}_L = [(1-\omega)\mathbf{D}_L + h_v(1-\omega_h)\mathbf{D}_{Lh}]^{-1} : [\mathbf{s}_{Lh} + h_v(1-\omega_h)\mathbf{D}_{Lh} : \boldsymbol{\varepsilon}_h] \tag{13}$$

Then, the local inelastic strain tensor ($\boldsymbol{\varepsilon}_\alpha$) is found by removing the elastic component of strain from $\boldsymbol{\varepsilon}_L$ (i.e. $\boldsymbol{\varepsilon}_\alpha = \boldsymbol{\varepsilon}_L - \boldsymbol{\varepsilon}_{Le}$, where $\boldsymbol{\varepsilon}_{Le} = \mathbf{C}_L : \mathbf{s}_{Lh}$). Thus, from (13), the additional local inelastic strain is given by:

$$\boldsymbol{\varepsilon}_\alpha = [(1-\omega)\mathbf{D}_L + h_v(1-\omega_h)\mathbf{D}_{Lh}]^{-1} : [\mathbf{s}_{Lh} + h_v(1-\omega_h)\mathbf{D}_{Lh} : \boldsymbol{\varepsilon}_h] - \mathbf{C}_L : \mathbf{s}_{Lh} \tag{14}$$

which is rearranged to group local stress and healing strain terms, as follows:

$$\boldsymbol{\varepsilon}_\alpha = \left[[(1-\omega)\mathbf{D}_L + h_v(1-\omega_h)\mathbf{D}_{Lh}]^{-1} - \mathbf{C}_L\right] : \mathbf{s}_{Lh} + \left[\frac{(1-\omega)}{h_v(1-\omega_h)}\mathbf{C}_{Lh} \bullet \mathbf{D}_L + \mathbf{I}^{2s}\right]^{-1} : \boldsymbol{\varepsilon}_h \tag{15}$$

where $\mathbf{I}^{2s}$ is the second order identity tensor, and $\mathbf{C}_{Lh} = \mathbf{D}_{Lh}^{-1}$.

The total inelastic strain tensor is obtained by integrating the contributions from (15) around a hemi-sphere, in the same way that the equivalent term was obtain in equation (2), giving the following:

$$\boldsymbol{\varepsilon}_{add} = \frac{1}{2\pi}\oiint_S \mathbf{N}_\varepsilon : \left(\left[[(1-\omega)\mathbf{D}_L + h_v(1-\omega_h)\mathbf{D}_{Lh}]^{-1} - \mathbf{C}_L\right] : \mathbf{s}_{Lh} + \left[\frac{(1-\omega)}{h_v(1-\omega_h)}\mathbf{C}_{Lh}\cdot\mathbf{D}_L + \mathbf{I}^{2s}\right]^{-1} : \boldsymbol{\varepsilon}_h\right) dS \tag{16}$$

The two components of equation (16) are now separated, as follows:

$$\boldsymbol{\varepsilon}_{at} = \frac{1}{2\pi}\oiint_S \boldsymbol{N}_\varepsilon \cdot \left[[(1-\omega)\mathbf{D}_L + h_v(1-\omega_h)\mathbf{D}_{Lh}]^{-1} - \mathbf{C}_L\right] : \boldsymbol{s}_{Lh} dS \tag{17}$$

$$\boldsymbol{\varepsilon}_{ah} = \frac{1}{2\pi}\oiint_S \mathbf{N}_\varepsilon \cdot \left[\frac{(1-\omega)}{h_v(1-\omega_h)}\mathbf{C}_{Lh}\cdot\mathbf{D}_L + \mathbf{I}^{2s}\right]^{-1} : \boldsymbol{\varepsilon}_h dS \tag{18}$$

The first term ($\boldsymbol{\varepsilon}_{at}$) gives the inelastic strain induced by the local stresses and the second term gives the total permanent strain due to cured healing agent.

The method used to evaluate $\boldsymbol{\varepsilon}_h$ is described in Section 2.3 and expanded upon in A ppendix B. The latter accounts for interactions between healed microcracks in different directions, which were not considered in the method proposed by Davies and Jefferson (2017).

The relationship between the total stress and strain tensors is derived by replacing $\boldsymbol{\varepsilon}_{add}$ in equation (1) with the two components from equations (17) and (18), as follows:

$$\sigma = \mathbf{D} : (\boldsymbol{\varepsilon} - \boldsymbol{\varepsilon}_{at} - \boldsymbol{\varepsilon}_{ah}) \tag{19}$$

The final steps in this derivation involve using equations (17) and (18) in equation (19), employing the static constraint (equation (20) and rearranging to obtain equation (21).

$$\mathbf{s}_{Lh} = \mathbf{N} : \boldsymbol{\sigma} \tag{20}$$

$$\sigma = \mathbf{D}_{sech} : (\boldsymbol{\varepsilon} - \boldsymbol{\varepsilon}_{ah}) \tag{21}$$

where $\mathbf{D}_{sech}$ is the equivalent secant stiffness tensor, as given below.

$$\mathbf{D}_{sech} = \left(\mathbf{I}^{4s} + \frac{\mathbf{D}}{2\pi}\cdot\left(\frac{1}{2\pi}\oiint_S \mathbf{N}_\varepsilon \cdot [\mathbf{A}^{-1} - \mathbf{C}_L]\cdot\mathbf{N} dS\right)^{-1}\cdot\mathbf{D}\right) \tag{22}$$

where $\mathbf{I}^{4s}$ is fourth order identity tensor and $\mathbf{A} = [(1-\omega)\mathbf{D}_L + h_v(1-\omega_h)\mathbf{D}_{Lh}]$.

2.3. Time dependent healing evolution

In this section, the method used to simulate the evolution of the healing variables is explained. This starts with a consideration of the relative proportion of material available to heal at a given time t, which is denoted by $a(t)$. It is assumed that healing agent is supplied instantaneously to any new microcracks and, thus, $a(t)$ increases at the same rate as $\omega(t)$, as follows:

$$\dot{a}(t) = \dot{\omega}(t) \tag{23}$$

in which the superior dot denotes the time derivative.

Healing occurs by healing-agent curing in microcracks. The function used to simulate the evolution of the degree of cure ($\phi \in [0,1]$) is taken from Freeman and Jefferson (2022, 2023), as follows:

$$\phi(t) = (1 - e^{-t_c/\tau}) \tag{24}$$

where τ is the curing time parameter, which depends on the chemical properties of the healing agent and the current curing time ($t_c = t - t_{c0}$).

With these assumptions, and in the absence of re-microcracking, the virgin healing variable at time t is given by the following convolutional integral:

$$h_v(t) = \phi_{he} \int_{s=t_{c0}}^{t} \frac{\partial a(s)}{\partial s} (1 - e^{-(\frac{t-s}{\tau})}) dS \tag{25}$$

where ϕ_{he} is a healing efficiency parameter.

The assumption that the degree of cure matches the degree of healing is different from that used in the macrocrack healing model of Jefferson and Freeman (2022), in which healing was computed from the overlap of curing fronts within a macrocrack. However, in microcracks with relatively small crack opening displacements, the degree of healing may be equated directly to ϕ.

Re-healing is simulated by a reduction in the re-microcracking variable (ω_h) such that the total proportion of healed material (h) at time t is:

$$h(t) = h_v(t)(1 - \omega_h(t)) \tag{26}$$

The relative proportion of material available for re-healing (a_r) is given by:

$$a_r(t) = h_v(t)\omega_h(t) \tag{27}$$

The re-healing variable is then obtained from:

$$h_r(t) = \phi_{he} \int_{t_{hr}}^{t} \frac{\partial a_r}{\partial s} (1 - e^{-t/\tau}) ds \tag{28}$$

where t_{hr} is the re-healing activation time.

The process of updating ω_h is best explained by considering a finite healing period from time t to $t + \Delta t_h$ and exploring the changes in the healing variables over that period. The increment of virgin healing Δh_v is computed from equation (29) using equation (25), the amount of re-healing Δh_r from equation (30) using equation (28), and ω_h by applying the healing increment to equation (26) to obtain equation (31) and rearranging to give equation (32):

$$\Delta h_v = \mathrm{h}_v(t + \Delta t_h) - \mathrm{h}_v(t) \tag{29}$$

$$\Delta h_r = \mathrm{h}_r(t + \Delta t_h) - \mathrm{h}_r(t) \tag{30}$$

$$(1 - \omega_h(t + \Delta t_h))h_v(t + \Delta t_h) = (1 - \omega_h(t))h_v(t) + \Delta h_v + \Delta h_r \tag{31}$$

$$\omega_h(t + \Delta t_h) = 1 - \frac{(1 - \omega_h(t))h_v(t) + \Delta h_v + \Delta h_r}{h_v(t + \Delta t_h)} \tag{32}$$

The representation of healing, re-microcracking and re-healing by equation (26) implies a homogenisation of material states across an RME. This is because the model does not track each separate directional component of micro-cracked and healed material that forms at a particular time; rather, these are grouped together and represented by a single virgin healing variable, a single microcracking variable and a single healing strain tensor (ε_h) for each microcracking direction. These microcracking and healing processes are illustrated in Fig. 3.

The next healing component that needs to be considered is the healing strain. As discussed in Section 2.2, the condition used to compute ε_h is that the state of stress should not change when healing alone occurs. If the local stress is considered and there is no change in

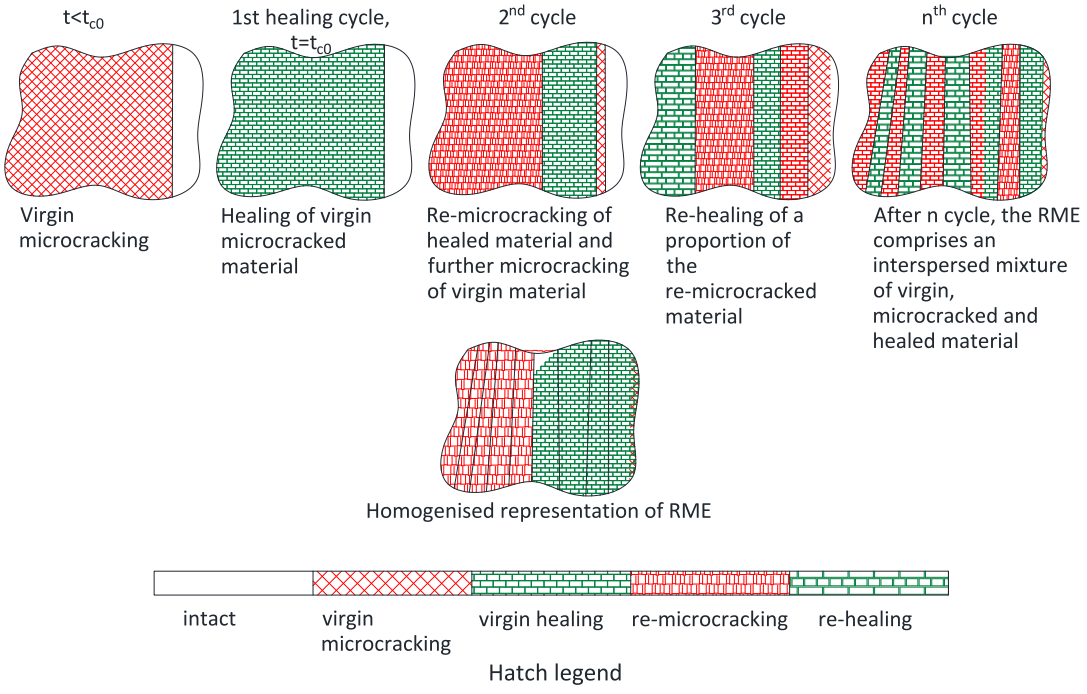

Fig. 3. Schematic representation of material states in successive microcracking and healing cycles.

either ω or $\boldsymbol{\varepsilon}_{\mathrm{L}}$ over the healing increment, then the zero change in the local stress condition may be written as follows:

$$\begin{aligned}\Delta\mathbf{s}_{\mathrm{Lh}} &= h_v(t+\Delta t_h)(1-\omega_h(t+\Delta t_h))\mathbf{D}_{\mathrm{Lh}} : (\boldsymbol{\varepsilon}_{\mathrm{L}} - \boldsymbol{\varepsilon}_{\mathrm{h}}(t+\Delta t_h)) \\ &= h_v(t)\big(1-\omega_{hp}\big)\mathbf{D}_{\mathrm{Lh}} : (\boldsymbol{\varepsilon}_{\mathrm{L}} - \boldsymbol{\varepsilon}_{\mathrm{h}}(t)) = 0\end{aligned} \tag{33}$$

where ω_{hp} is the microcracking variable at the start of the healing sub-step.

Then, the change in the value of ε_{h} at the end of the healing increment may be deduced to be:

$$\boldsymbol{\varepsilon}_{\mathrm{h}}(t+\Delta t_h) = \frac{h_v(t+\Delta t_h)(1-\omega_h(t+\Delta t_h))\boldsymbol{\varepsilon}_{\mathrm{L}} - h_v(t)\big(1-\omega_{hp}\big)(\boldsymbol{\varepsilon}_{\mathrm{L}} - \boldsymbol{\varepsilon}_{\mathrm{h}}(t))}{h_v(t+\Delta t_h)(1-\omega_h(t+\Delta t_h))} \tag{34}$$

This update ignores the interaction between local directions and means that if ε_{h} from equation (34) were to be used directly in equation (18) the condition that the total stress remains constant over a healing increment would not be guaranteed. The solution to this problem involves the introduction of an interaction factor (α_j) for each microcracking direction (j), as explained in Appendix B. These interaction factors modify the contribution of each local healing strain tensor ($\boldsymbol{\varepsilon}_{\mathrm{h}}$) to the total healing tensor $\boldsymbol{\varepsilon}_{\mathrm{ah}}$. The modified $\boldsymbol{\varepsilon}_{\mathrm{ah}}$ tensor is denoted $\boldsymbol{\varepsilon}_{\mathrm{Gh}}$ (see equation (B.8) and is given by:

$$\boldsymbol{\varepsilon}_{\mathrm{Gh}} = \mathbf{C}\alpha\boldsymbol{\varepsilon}_{\mathrm{h}} \tag{35}$$

The expression in equation (35) then replaces $\boldsymbol{\varepsilon}_{\mathrm{ah}}$ in equation (21), as follows:

$$\boldsymbol{\sigma} = \mathbf{D}_{\mathrm{sech}} : (\boldsymbol{\varepsilon} - \boldsymbol{\varepsilon}_{\mathrm{Gh}}) \tag{36}$$

The final aspect of the management of the healing variables is the update of the healing strain parameter (ζ_h) to account for the change in ω_h due to healing. This is obtained by solving the following nonlinear equation which is derived by equating $\omega_h(t+\Delta t_h)$ from equation (32) to the expression for ω_h given in equation (11), as follows:

$$solve\ \omega_h(t+\Delta t_h) - \left(1 - \frac{\varepsilon_t}{\zeta_h} e^{-c\left(\frac{\zeta_h(t+\Delta t_h)-\varepsilon_{ht}}{\varepsilon_{h0}-\varepsilon_{ht}}\right)}\right) = 0 \text{ for } \zeta_h(t+\Delta t_h) \tag{37}$$

2.4. Update algorithm for healing variables

The numerical solutions used for the above equations are now considered. Firstly, h_v and h_r are defined by the convolution integrals given in equations (25) and (28) respectively, which may be solved conveniently by using a standard two-level recursive scheme (Simo and Hughes, 1998; Mergheim and Steinmann, 2013). The resulting expressions for h_v and h_r are as follows, noting that times t and $t+\Delta t_h$ are now denoted by subscripts i and $i+1$respectively:

$$h_{v_{i+1}} = h_{v_i} e^{-\frac{\Delta t_h}{\tau}} + \phi_{he} a_{i+1}\left(1 - e^{-\frac{\Delta t_h}{\tau}}\right) \tag{38}$$

$$h_{r_{i+1}} = h_{r_i} e^{-\frac{\Delta t_h}{\tau}} + \phi_{he} a_{r\,i+1}\left(1 - e^{-\frac{\Delta t_h}{\tau}}\right) \tag{39}$$

Each time step is sub-divided into a microcracking sub-step and a healing sub-step. The solution is quasi-static such that no inertia terms are included, and it is assumed that any changes to the microcracking field occur instantaneously at the start of each time step. Healing is then considered to occur over the time step, starting from the current state of microcracking. Thus, the healing sub-step (Δt_h) is the same duration as the overall time step (Δt).

The algorithm developed for computing the stress and updating the microcracking and healing variables at a particular timestep is given in Algorithm box 1. The primary directional microcracking and healing variables/tensors to be updated are $\zeta, \zeta_h, \omega_h, h_v$ and $\boldsymbol{\varepsilon}_h$. The dependent variables include ω&h_r. It is noted that ω_h is a dependent variable during a microcracking sub-step but is updated directly during a healing sub-step. In the latter, ζ_h is updated according to the new value of ω_h .

The vectors containing the values from all directions are denoted with bold non-italic text. The values from a previous step, or sub-step, are denoted with the subscript p.

The integration over the hemispherical domain is evaluated numerically using MacLaurin's 29 point integration rule (i.e. $n_d = 29$) (Stroud, 1973). These directions and the associated integration weights are given in A ppendix A. For convenience, Voigt notation is used in the description of algorithm 1.

Algorithm 1 Computational algorithm.

The starting variable values for all directions from the previous time step (null if first step) $\boldsymbol{\zeta}_{\mathrm{p}}, \boldsymbol{\zeta}_{\mathrm{hp}}, \mathbf{h}_{\mathrm{vp}}$ & $\boldsymbol{\varepsilon}_{\mathbf{hp}}$ and the total stress ($\boldsymbol{\sigma}$) to be updated for the new total strain $\varepsilon + \Delta\varepsilon$, for time t to $t + \Delta t$, noting that $\Delta t = \Delta t_h$

Mechanicalsub −step

forj $= 1 to n_d$ Loop over spherical integration directions (see App. A for integration directions and weights)

$\varepsilon_{L_j} = \mathbf{N}_{\varepsilon_j}(\varepsilon + \Delta\boldsymbol{\varepsilon})$) Calculate local strain tensor

$\zeta_{ef}(\boldsymbol{\varepsilon}_{Lj})$&$\zeta_{h_{ef}}\left(\boldsymbol{\varepsilon}_{Lj} - \boldsymbol{\varepsilon}_{hp_j}\right)$ Find effective strains for original and healed material (eq. 5&12)

Update $\zeta_j(\zeta_{ef_j}, \zeta_{p_j}), \zeta_{hj}(\zeta_{h_{ef}}, \zeta_{hp_j}), \omega_j(\zeta_j), \omega_{hj}(\zeta_{hj})$ Update local microcracking parameters and variables for original material (eq. 5–7) & healed material (eq. (11)–(12)

$\Delta\omega_j = \omega_j - \omega_{p_j}$&$\Delta\omega_j = \omega_{hj} - \omega_{hp_j}$ Compute the increments of the microcracking variables for original and healed material

$h_{r_j} = h_{v_{p_j}}\left(1 - \omega_{h_j}\right)$ Update the re-healing variable for microcracking

$\mathbf{A}_j = \left[(1-\omega_j)\mathbf{D}_{\mathrm{L}} + h_{v_{p_j}}\left(1-\omega_{h_j}\right)\mathbf{D}_{\mathrm{Lh}}\right]$ Compute the local microcracking – healed constitutive tensor (see line below eq. (22)

endjloop Close loop over integration directions

$\boldsymbol{\zeta_{hp}} = \boldsymbol{\zeta_h}; \boldsymbol{h_{v_p}} = \boldsymbol{h_v}; \boldsymbol{h_{r_p}} = \boldsymbol{h_r}$

$\boldsymbol{\omega_{hp}} = \boldsymbol{\omega_{hp}}(\boldsymbol{\zeta_{hp}})$ Record values of healing and re-microcracking variables that have been updated for new microcracking.

Healing sub-step, if healing is active If healing is activated continue, else jump to end of section.

forj $= 1 to n_d$ Loop over spherical integration directions

$a_j = a_{p_j} + \Delta\omega_j$

$a_{rj} = a_{r_{p_j}} + \Delta h_{v_{p_j}}\omega_{hp_j}$ Calculate proportions of material available for healing (eq. (23) and re-healing (eq. (27)

$h_{v_j} = h_{v p_j} e^{\frac{-\Delta t}{\tau}} + a_j\left(1 - e^{\frac{-\Delta t}{\tau}}\right)$

$h_{r_j} = h_{r_{p_j}} e^{-\frac{\Delta t}{\tau}} + \phi_{he} a_{rj}\left(1 - e^{-\frac{\Delta t}{\tau}}\right)$

$\Delta h_{vj} = h_{v_j} - h_{v p_j}$

$\Delta h_{rj} = h_{r_j} - h_{r_{p_j}}$ Update the virgin healing and re-healing variables (eqs. (38) & (39) along with their increments (eqs. (29) & (30)

$\omega_{hj} = 1 - \frac{\left(1-\omega_{hp_{j_j}}\right)h_{v p_j} + \Delta h_{vj} + \Delta h_{rj}}{h_{vj}}$ Update the healed material microcracking variables due to re-healing. (eq. (32)

$Solve \omega_{hj} - \left(1 - \frac{\varepsilon_t}{\zeta_{hj}} e^{-c\left(\frac{\zeta_{hj}-\varepsilon_{ht}}{\varepsilon_{h0}-\varepsilon_{ht}}\right)}\right) = 0$

for ζ_{hj}

Update the nonlinear equation for the microcracking strain parameter for healing. (eq. (37)

(*continued on next page*)

(*continued*)

$\varepsilon_{\mathrm{h}j} = \dfrac{h_{vj}(1-\omega_{hj})\varepsilon_{\mathrm{L}j} - h_{vj}(1-\omega_{hp_j})\left(\varepsilon_{\mathrm{L}j} - \varepsilon_{\mathrm{h}p_j}\right)}{h_{vj}(1-\omega_{hj})}$ Compute the current local healing strains (eq. (34)

$\mathbf{A}_j = \left[(1-\omega_j)\mathbf{D}_{\mathrm{L}} + h_{vj}\left(1-\omega_{h_j}\right)\mathbf{D}_{\mathrm{Lh}}\right]$ Update the local microcracking – healed constitutive tensor (eq. (22)

endjloop Close loop over integration directions

End if: *active healing*

$\mathbf{D}_{\mathrm{sech}} = \left(\mathbf{I} + \dfrac{\mathbf{D}_{\mathrm{el}}}{2\pi}\sum_{j=1}^{n_d}\mathbf{N}_{\mathrm{ej}}^{\mathrm{T}}\left[\mathbf{A}_j^{-1} - \mathbf{C}_{\mathrm{L}}\right]\mathbf{N}_j w_{dj}\right)^{-1}\mathbf{D}_{\mathrm{el}}$ Update the secant stiffness (eq. (22)

$\boldsymbol{\varepsilon}_{\mathrm{Gh}} = \mathbf{C}\alpha\boldsymbol{\varepsilon}_{\mathbf{h}}$

$\sigma = \mathbf{D}_{\mathrm{sech}}(\boldsymbol{\varepsilon} - \boldsymbol{\varepsilon}_{\mathrm{Gh}})$ Update the total healing strain tensor, allowing for interactions (eq (35) and A ppendix B), noting that the vector $\boldsymbol{\varepsilon}_{\mathbf{h}}$ contains the stacked local healed strain vectors $\varepsilon_{\mathrm{h}j}$ for all local directions $j = 1$ to n_d

Compute the total stress.

end

The schematics in Fig. 3 illustrate the changing state of material during successive microcracking-healing cycles within an RME, and the homogenised representation of the RME based on equation (26).

The new micromechanics based self-healing constitutive model was implemented in a finite element code developed at Cardiff University. A standard virtual work formulation was adopted to evaluate the stiffness matrix. Material nonlinearity was considered, and the domain was assumed to be continuous throughout the loading history. The nonlinear system of equations is solved using a standard Newton incremental iterative scheme.

3. Single point simulations

A series of single-point simulations is presented in this section in order to illustrate the performance of the proposed constitutive model. The material properties such as the modulus of elasticity (E), tensile strengths (f_t) and Poisson's ratio for original and healed materials (denoted by subscript h) that used for the simulations are given in Table 2. The first example replicates a uniaxial tensile test with an applied strain rate of 5×10^{-6} /s in the xx-direction. The simulations were undertaken for a range of curing time parameters (see τ range in Table 2) and healing scenarios. The latter comprise no-healing (Nh), single healing (Sh) and multiple healing (Mh) scenarios. 'Multiple healing' means that the mechanism within the model to simulate an unlimited number of simultaneous microcracking and healing steps is active.

The overall responses for each scenario, along with the associated evolutions of the microcracking variables, are given in Fig. 4.

In this example, healing was assumed to commence when the strain reached 0.003. For the material properties given, this strain value would be associated with substantial microcracking in a real self-healing material and is approximately 70 times greater than the crack initiation strain. It is noted that the healing activation criterion varies

Table 2
Material properties.

Variables	$E(N/mm^2)$	$E_h(N/mm^2)$	ν, ν_h	$f_t, f_{th}(N/mm^2)$	$\tau(s)$	$\varepsilon_0, \varepsilon_{0_h}$
Properties	24,000	12,000	0.15	1	1–60-200	0.0067

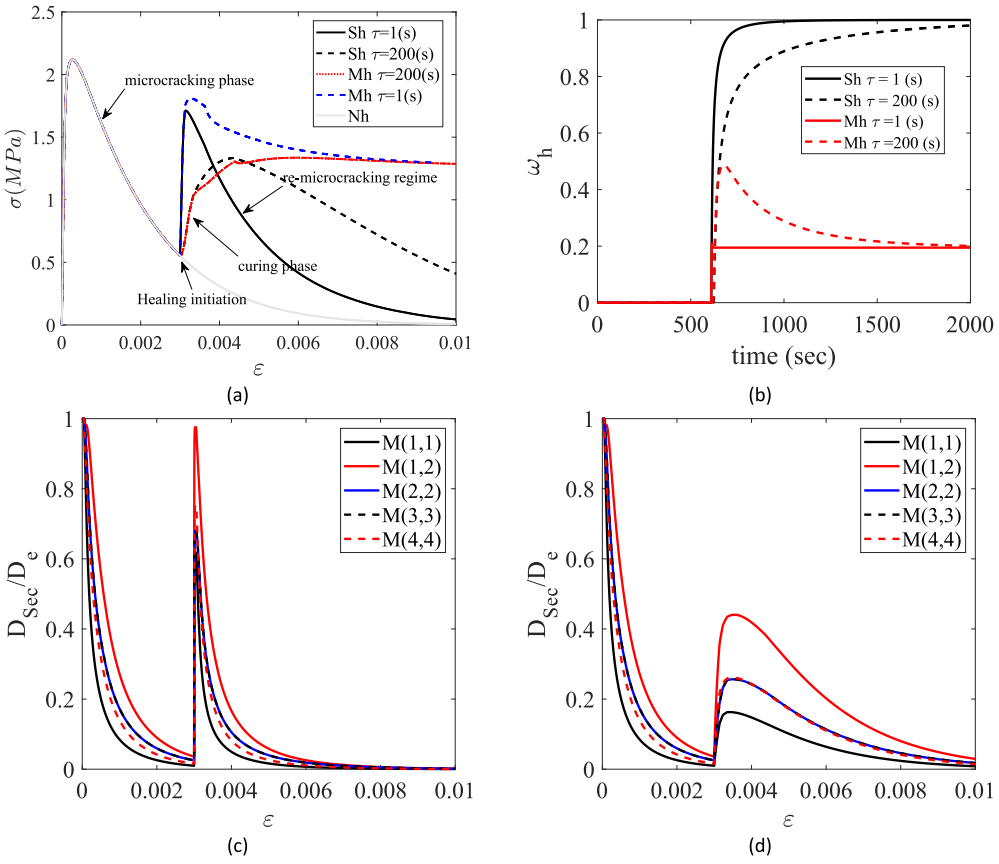

Fig. 4. Computed uniaxial responses, a) variation of stress with time, b) re-microcracking variables, c) Stiffness matrix component for $\tau = 1s$ and d) stiffness matrix component for $\tau = 200s$.

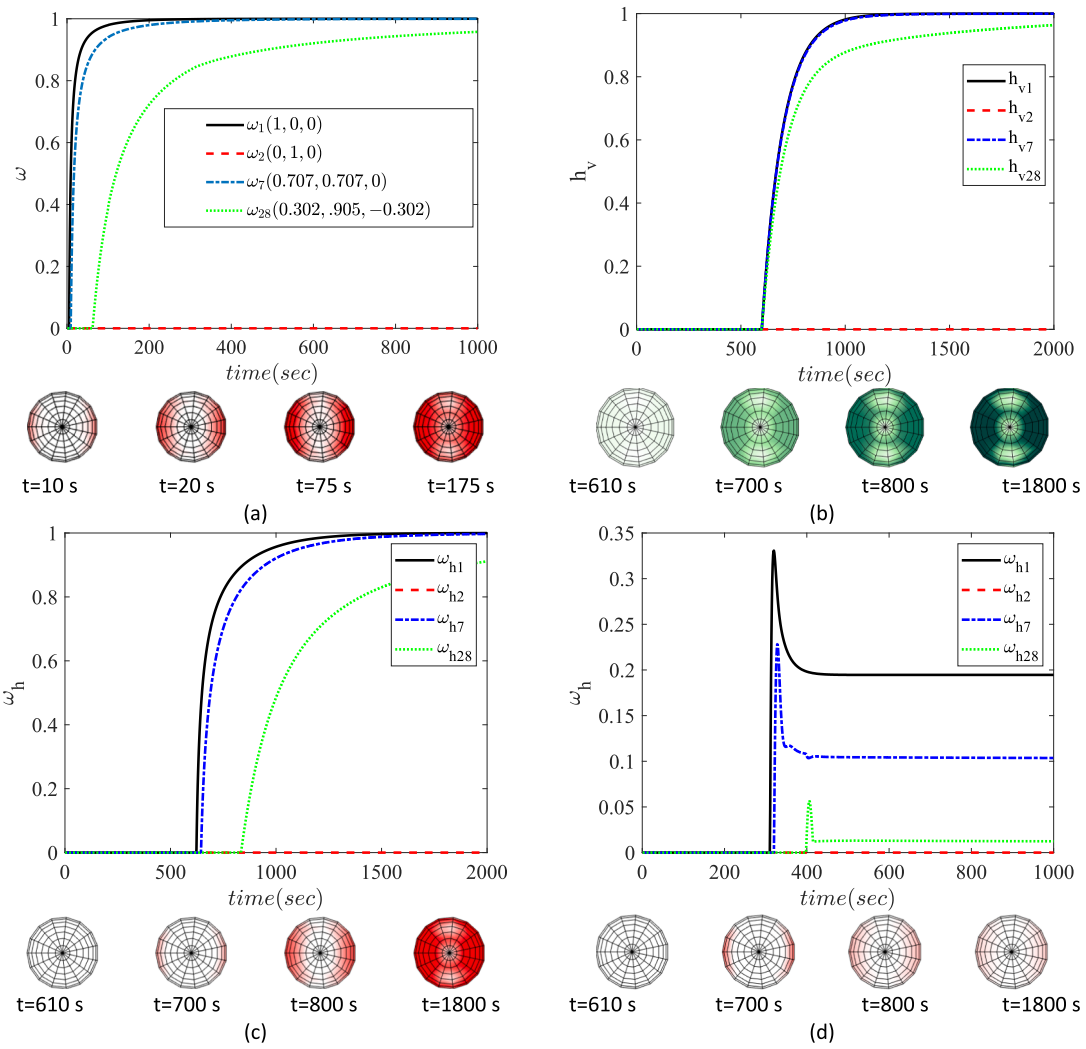

Fig. 5. Microcracking and healing variable evolution, a) virgin microcracking b) virgin healing, c) re-microcracking for single healing cycle and d) re-microcracking-re-healing variables for multiple healing cycles.

considerably with the type of healing system and with the properties of the host material.

The results show that the response is strongly affected by the value of the curing time parameter with the healing response being less abrupt for larger values of τ. It is noteworthy that the responses of the three healed material simulations tend to the same asymptotic stress, which is associated with balanced healing and microcracking rates. Furthermore, the ability of the model to capture anisotropic behaviour is explored by considering the changes to the components of the stiffness tensor over the prescribed strain path. The secant stiffness tensor (in Voigt matrix form) is normalised with the elasticity tensor (matrix), such that $\mathbf{M} = \mathbf{D}^{-1}\mathbf{D}_{\text{sech}}$. The component numbers shown in Fig. 4c and 4d are selected matrix terms in Voigt notation. The changes in these matrix terms are illustrated in Fig. 4c and d for $\tau = 1$ and 200 (s) respectively. The results show that the relative matrix terms change in an anisotropic manner as microcracking and healing progress.

In order to provide more insight into the anisotropic behaviour of the model, the variation of the microcracking and healing variables for four selected directions have been plotted for all three healing scenarios for the $\tau = 60s$ case in Fig. 5. The direction numbers correspond with the spherical integration directions given in Appendix A.

As may be expected, the maximum microcracking occurs in direction 1 which coincides with the loading direction. The microcracking variable in direction 1 (i.e.ω_1) has a value of 0.99 at the time healing initiates; by contrast, the corresponding value of $\omega_{28} = 0.90$. The ω values for the directions that do not correspond with the loading direction illustrate the effect of the local shear strains, as well as the local normal strains, on the degree of microcracking around the hemisphere. As may be expected, the progression of the microcracking and healing responses for the non-coincident directions lag those of direction 1, with the lag increasing as the angle between direction 1 and the normal to the local direction under consideration increases. The microcracking and healing variables are visualised in the polar plots shown in Fig. 5. These polar plots are given at times 10, 20, 75 and 175 s for the microcracking variables and 610, 700, 800 and 1800 s for the healing and re-microcracking variables.

3.1. Parametric study

The results of a systematic parametric study are now presented in which the model was used to predict the uniaxial response of a self-healing cementitious sample. The reference properties are those given in Table 2. The material properties altered sequentially in the study were the curing time, healed material Young's modulus and healed material strength. The sequence of values used for each parameter are given in Table 3. The range of healing scenarios considered are as follows:

Table 3
Material properties for parametric study.

Case/material properties	Ranges	τ(sec)	E_h(N/mm^2)	f_{th}(N/mm^2)
τ	1, 10, 50, 100, 400	variable	12,000	1
$E_r = E_h/E^*$	0.25, 0.5, 1, 1.5, 2	50	variable	1
$f_r f_{th}/f_t$**	0.25, 0.5, 1, 1.5, 2	50	12,000	variable

* Er denotes the ratio of the elastic modulus of healing material to original material.
** fr denotes the ratio of the tensile strength of healing material to original material.

i) single healing under continuous monotonic loading ($\dot{\epsilon} = 5 \times 10^{-6}$ /s):
ii) multiple microcracking-healing under continuous monotonic loading ($\dot{\epsilon} = 5 \times 10^{-6}$ /s):
iii) multiple microcracking-healing events under loading–unloading-reloading conditions (loading $\dot{\epsilon} = 5 \times 10^{-6}$; unloading $\dot{\epsilon} = -5 \times 10^{-6}$; reloading rate varies as shown in Fig. 6)

Fig. 6 presents the predicted mechanical response for all of the cases considered. The relative effect of changing each parameter in turn is evident from the graphs, with changes in the healed-material strength and stiffness greatly affecting the post-healed peak load and post-peak softening response. As already mentioned, changing τ has a profound influence on the apparent stiffness and ductility of the post-healed response, with lower values of τ being associated with lower post-healed peak strengths and an apparent more ductile response.

For real cases, the model parameters are calibrated by using experimental data from uniaxial microcracking tests to determine the softening parameters of equation (7), such that the peak and post-peak behaviour are captured accurately. Then, the healing-efficiency parameter (ϕ_{he}) is found using data from uniaxial microcracking – healing tests, with ϕ_{he} being calibrated such that the computed overall stiffness recovery matches the corresponding experimental value. The healing activation time is obtained through direct observation. These microcracking and healing parameters are variable since they depend on the mechanical properties of the overall self-healing system, as well as those of the components, such as microcapsule shells and vascular network channels.

3.2. Microencapsulated uniaxial test

The proposed model's ability to replicate the mechanical response of samples formed from a self-healing cementitious material containing microcapsules is assessed by considering the experimental tests on a set of cylindrical samples undertaken by James et al. (2014). In this work, the investigators measured the effects of healing on the elastic modulus of a microencapsulated self-healing cementitious material system. The tests considered material samples formed with 400–500 μm sized microcapsules containing sodium silicate at dosages of 0.5 % and 1 % by volume of the cement paste. The tests followed a procedure from ASTM C469 for measuring the static elastic modulus. Each cylindrical sample was loaded axially up to 70 % of the nominal compressive strength in order to induce a degree of microcracking. The samples were then unloaded and allowed to heal for 3 days and then reloaded to failure.

The material properties used for the simulations are presented in Table 4.

Table 4
Material properties.

Material/properties	$E(N/mm2)$	ν	$f_t(N/mm2)$	ε_0
Matrix	32,430	0.25	1	0.0025
Capsule	3000	0.2	–	
Healing agent	3000	0.2	5	0.0003

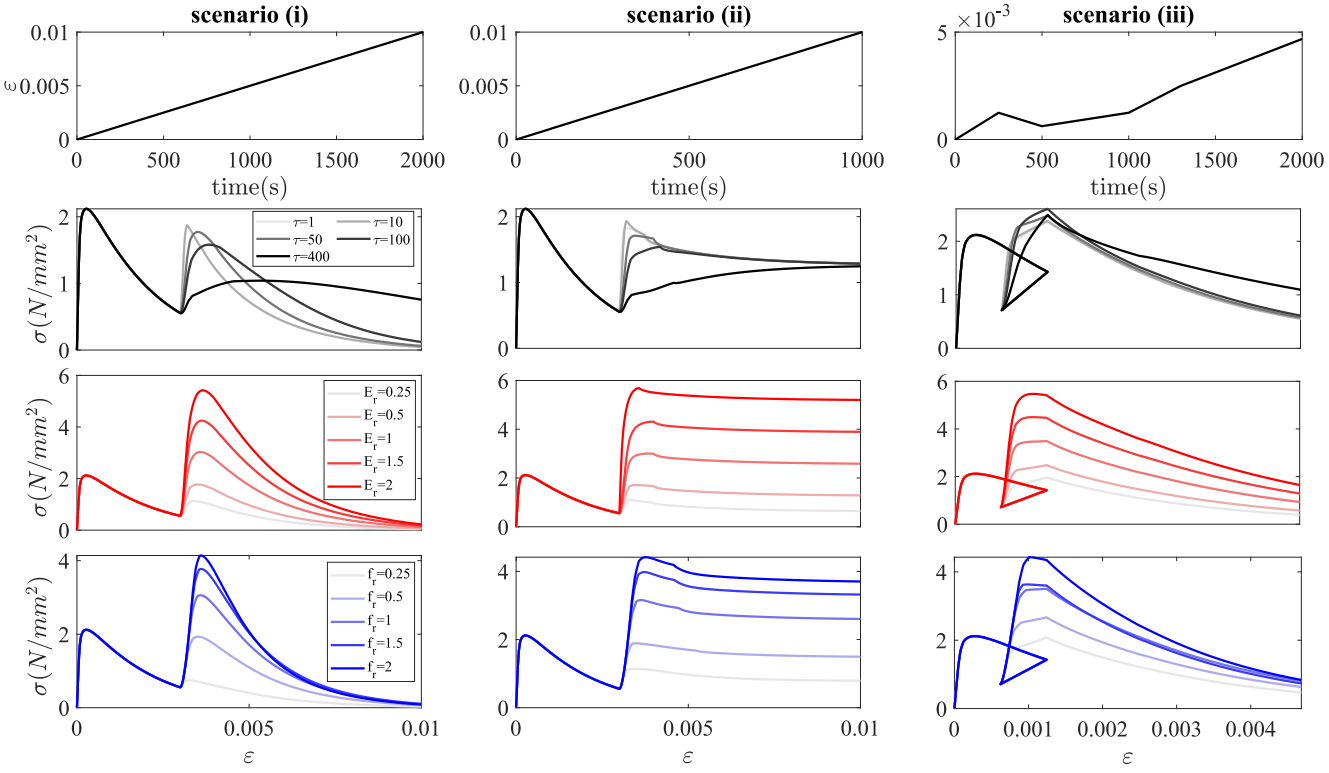

Fig. 6. Parametric study results.

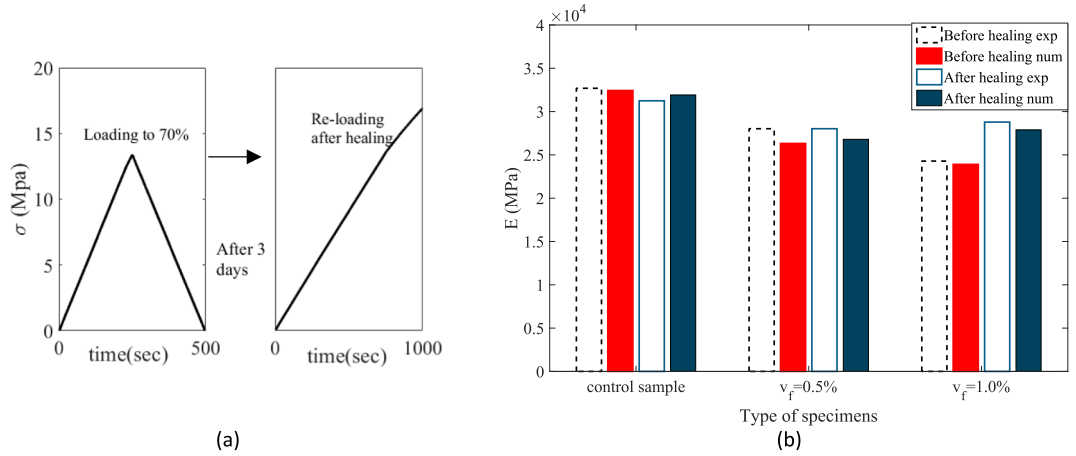

Fig. 7. Experimental validation, a) loading protocol, b) stiffness recovery comparison.

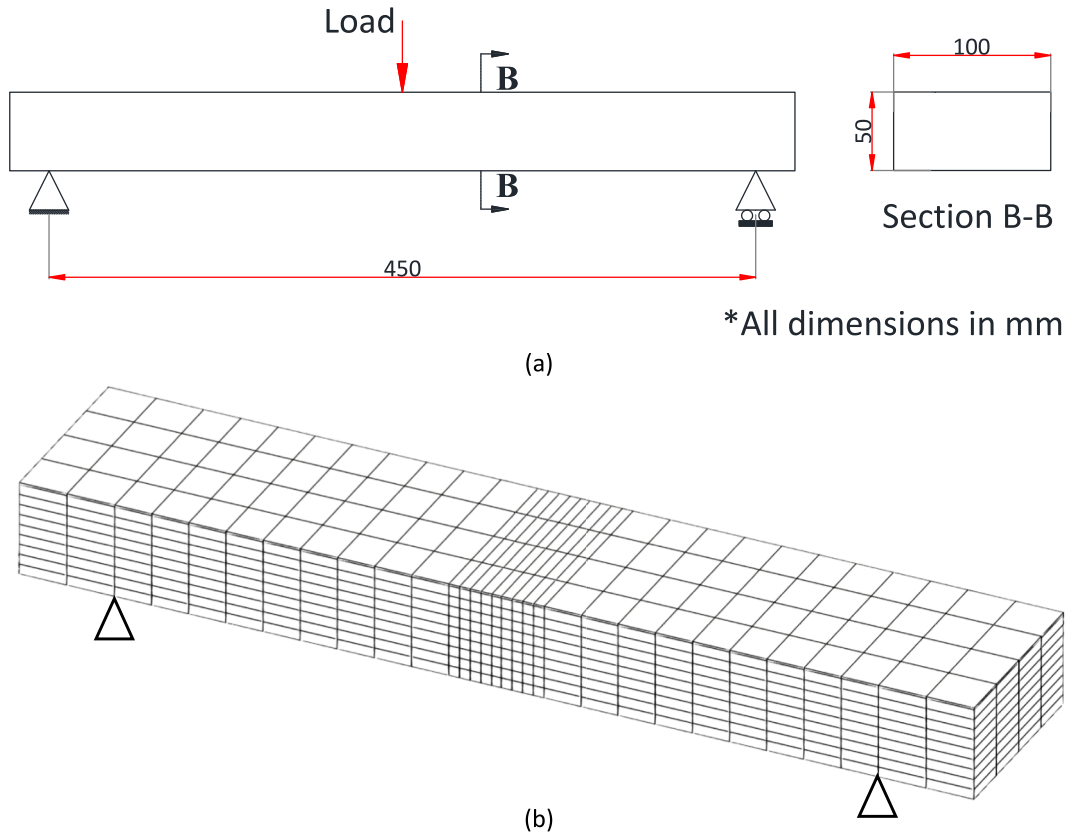

Fig. 8. (a) Beam geometry and boundary conditions, b) finite element mesh.

The results of the simulations are presented in Fig. 7, with Fig. 7a giving the loading protocol and Fig. 7b the experimental and numerical values of the elastic moduli before and after healing for each case. It is evident from the differences between the initial stiffnesses of the control samples and the samples containing microcapsules that the presence of the microcapsules reduced the stiffness of the material.

The results of the samples with microcapsules shows that the model is able to reproduce the increase in stiffness brought about by healing, and to capture the effect of increasing the dosage of microcapsules. It is noted that the experimental data did not include any load–displacement responses.

4. Finite element example: Self-healing beam tests

The 3-point beam bending experiments conducted by Ferrara et al. (2014) are considered in this example. In these experiments, concrete beams of size 450 × 100 × 50 mm (Fig. 8a), were cast and loaded until the crack mouth opening displacement (CMOD) reached 150 μm and 300 μm for first and second healing cycle respectively. Some of these beams were formed from a standard concrete mix and others were formed with a concrete containing a proprietary crystalline admixture (CA) (Ferrara et al. 2014), which was assumed to act as an autogenous healing enhancer. Ater cracking, each sample was stored for 12 months in either, (i) dry air or (ii) a water curing tank. The beams were then re-loaded until failure. The cases considered are summarised in Table 5.

The material properties used for the simulations (see Table 5) were

Table 5
Material properties used for bvp simulation.

Case/ parameter	Curing condition	Name	$E, E_h (N/mm^2)$	ν, ν_h	$f_t\ (N/mm^2)$	$f_{th}\ (N/mm^2)$	τ(days)	ϕ_{he}	$\varepsilon_0, \varepsilon_{0h}$
Healing without CA	Dry	WCAD	35,000	0.25	0.1	0.5	270	0.01	0.0025
Healing without CA	Wet	WCAW	35,000	0.25	0.3	0.5	270	0.02	0.0025
Healing with CA	Dry	CAD	35,000	0.25	0.45	0.5	135	0.08	0.0025
Healing with CA	wet	CAW	35,000	0.25	0.5	0.5	135	0.1	0.0025

based on those reported by Di Luzio et al. (2018); Ferrara et al. (2014) and Cibelli et al. (2022). The beam was modelled with the finite element program containing the new constitutive model. The testing arrangement, specimen geometry, boundary conditions and finite element mesh used for the analysis are illustrated in Fig. 8.

The simulations of the control specimens (without CA) only considered the first healing cycle, since no appreciable healing was observed in the second cycle. By contrast, the second healing cycle was considered

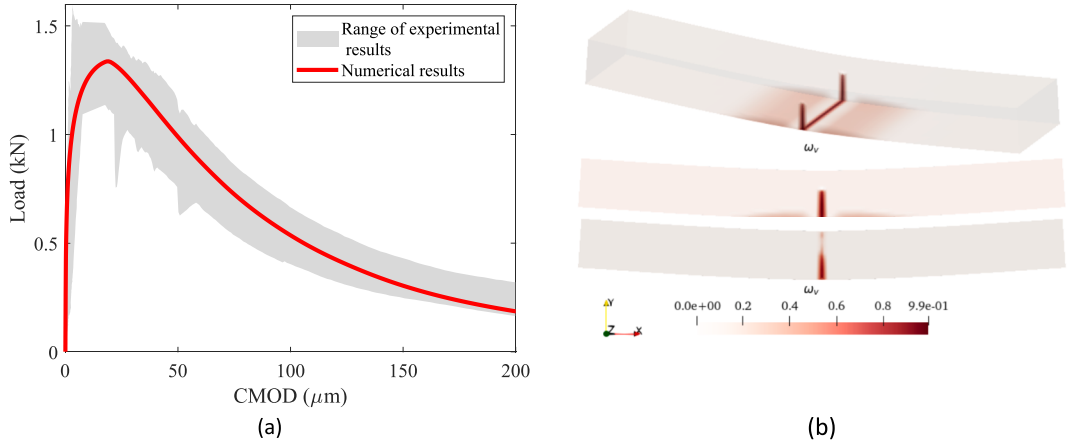

Fig. 9. Experimental and numerical control beam responses, a) load v CMOD response, b) microcracking variables at a CMOD of 150 μm.

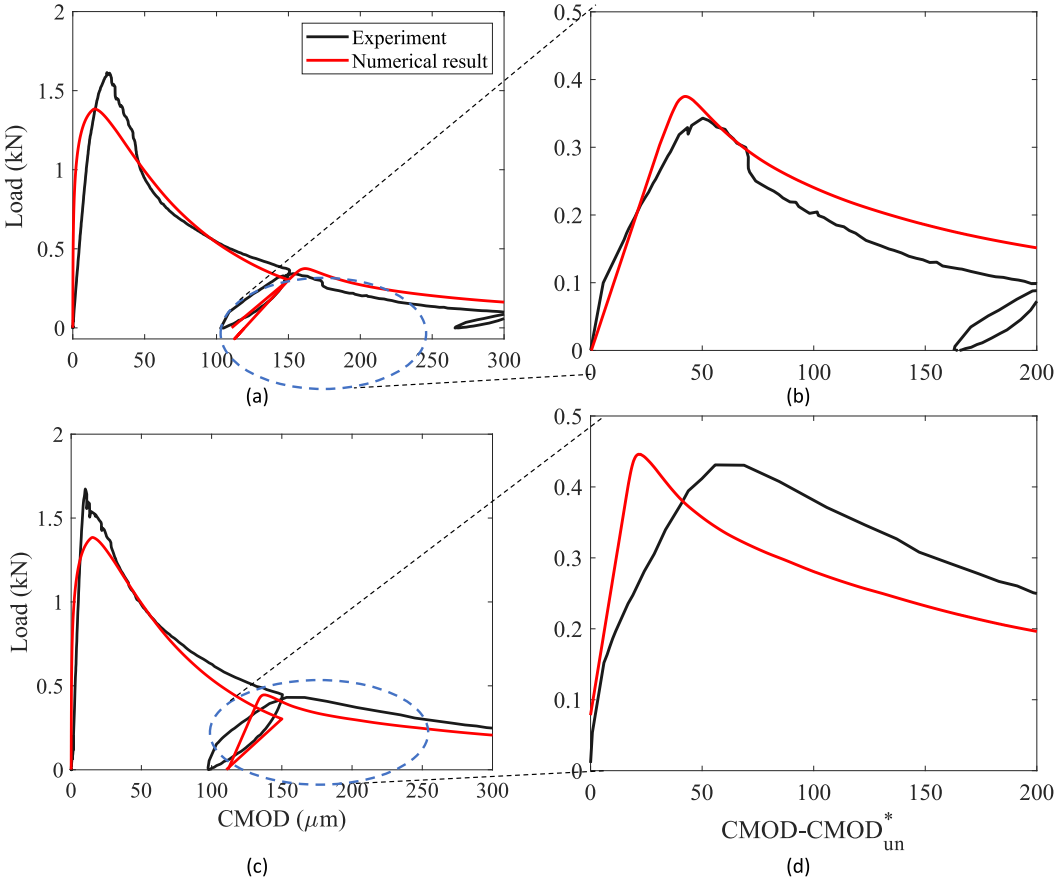

Fig. 10. Load-CMOD response for WCAD samples (a-b) and WCAW (c-d), a) loading −reloading response with healing, b) magnified illustration of (a), c) reloading with healing for WCAW, and d) magnified illustration of (c).

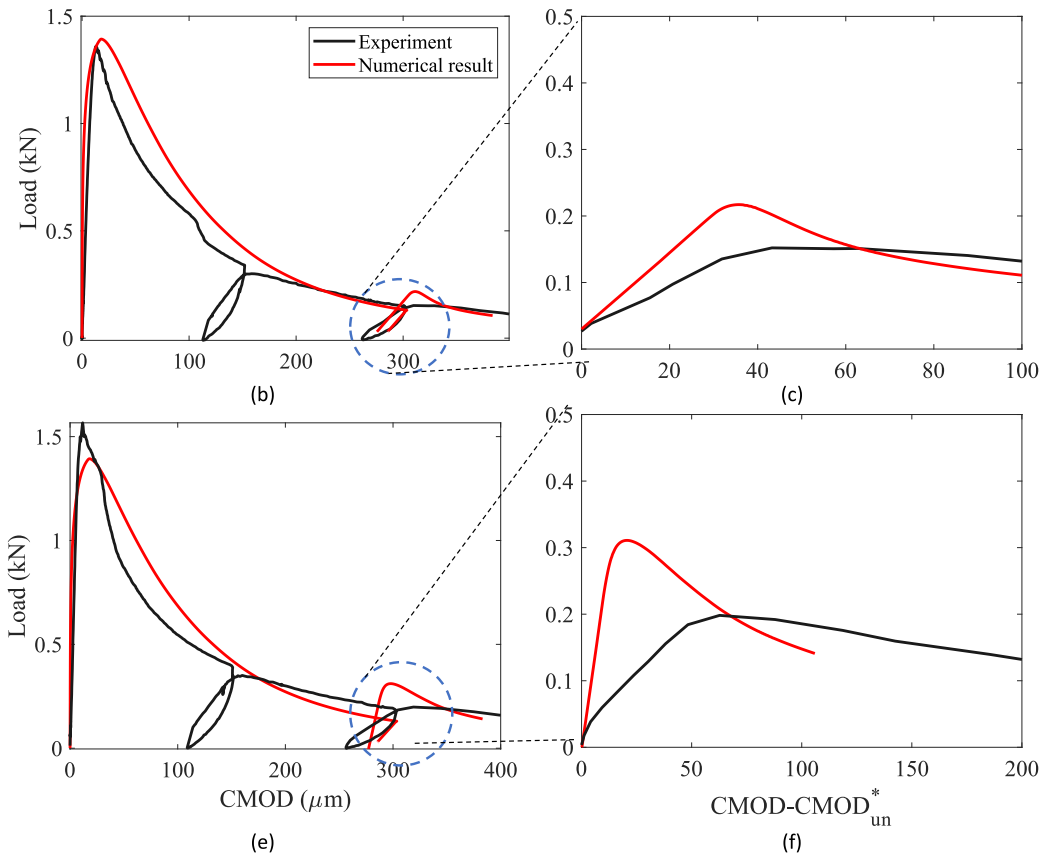

Fig. 11. Load-CMOD response for samples with CA cured in dry (CAD) (a-b) and wet conditions (c-d) (CAW), a) loading reloading process with healing for CAD, b) magnified illustration of (a), c) Loading reloading with healing for CAW and d) magnified illustration of (c).

for the specimens with CA. This is because negligible healing was observed in the first cycle for the CA samples, but significant healing was measured for the second cycle.

The experimental and numerical responses of the control samples are given in Fig. 9, which also shows the distribution of selected microcracking variables. The results show that the model is able to simulate the overall response of the control specimens with good accuracy.

The mean experimental and numerical load-CMOD responses, for the samples without and with CA, are given in Fig. 10 and Fig. 11 respectively. In these graphs, the post-curing reloading response commences from the unloading point of the initial cracking stage.

Comparing Fig. 10b and c with 10e and f, shows that the stiffness and strength recoveries due to healing were significantly less for dry cured specimens than for the wet-cured specimens without CA. The model captures this difference, although does show a small increase in post-healed strength for the dry specimens that was not evident in the corresponding 'wet' experiments. However, in wet conditions the strengths increased up to 10 %. The effect of CA on mechanical recovery shows itself in both strength and stiffness regains, as illustrated in Fig. 11 c and f.

Fig. 12 gives plots that show the distribution of the healing and re-microcracking variables at selected stages of the analysis for the CAW case. Fig. 12a shows that, at the start of reloading stage, the healed material re-microcracking value is zero, since at this point the healed material has just formed in a stress-free condition. It subsequently experiences microcracking. Re-microcracking values for the normal crack direction are shown in Fig. 12 b and c for CMOD values of 310 and 350 μm respectively. This figure also shows that the further microcracking is localised where healing material was formed.

5. Conclusions

A new micromechanical model for simulating the response of self-healing cementitious materials has been presented in this paper. The proposed constitutive formulation captures the time-dependent behaviour of these materials with good accuracy using relatively few physically meaningful material parameters.

The model simulates microcracking and its healing using the assumption that all microcracked material has the potential to be healed. The micromechanical formulation is well suited to simulating distributed cracking and healing for systems in which the healing material is spread throughout the structural element. This applies to healing systems that use embedded microcapsules. The model is not aimed at simulating discrete cracks or systems that use vascular networks, although some aspects of the behaviour of the latter can be captured by the model.

The constitutive model was implemented in a 3D finite element framework for simulating boundary value problems. Based on the results, the following conclusions can be drawn:

- the mechanical properties of healed material −often a healing-agent cementitious-matrix composite- greatly affect the post-cracking mechanical response of self-healing materials:
- the recursive scheme used to update the healing and re-cracking variables is an effective way to simulate the response of elements

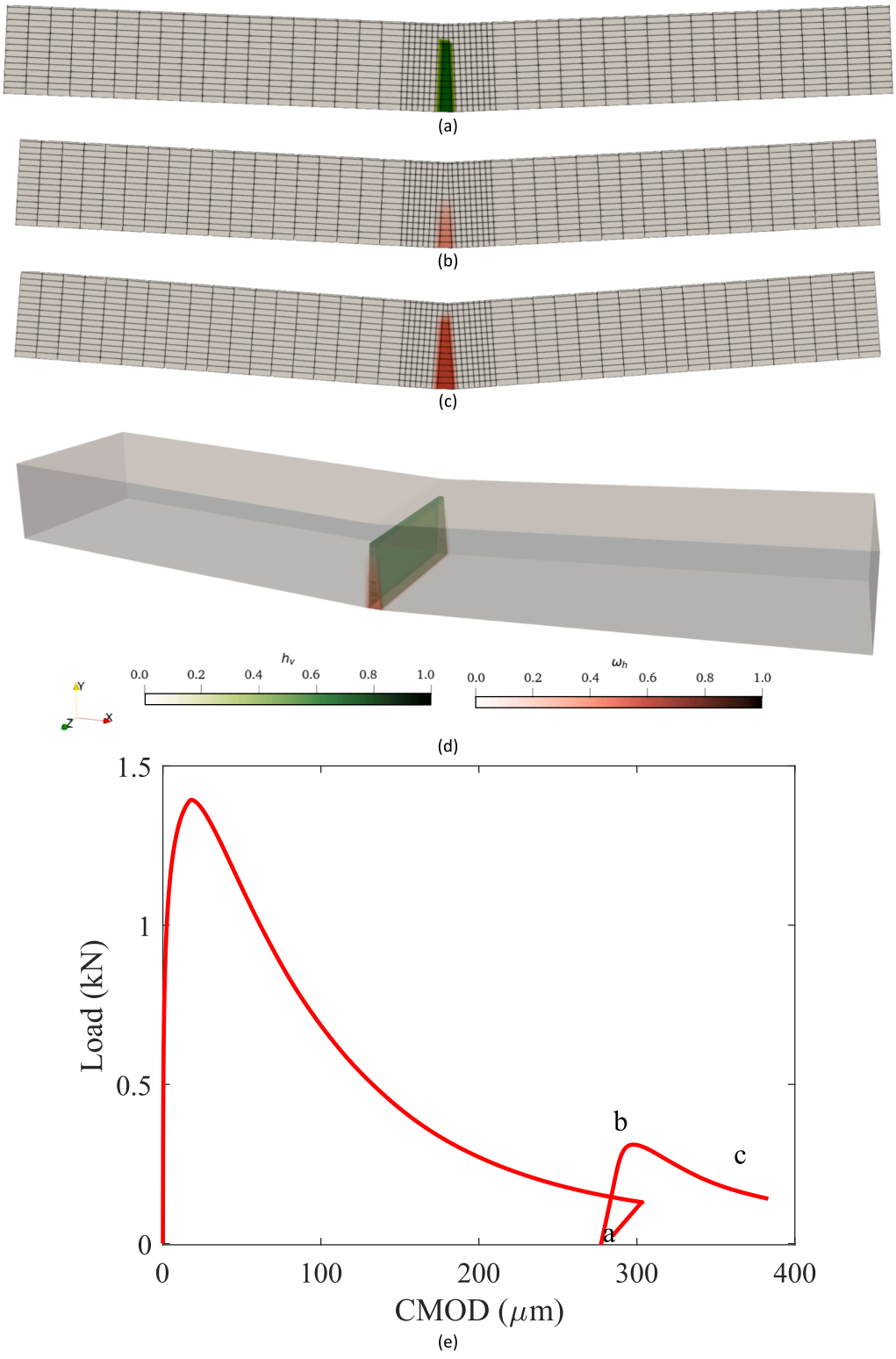

Fig. 12. Healed material status after reloading a) healing at CMOD = 275 μ m, b) re-microcracked at CMOD = 310 μ m c) re-cracking at CMOD = 350 μ m, d) overlapping cracking and healing illustration, and e) load-CMOD response for CAW.

to multiple and continuous microcracking-healing cycles in a computationally efficient manner:

- the model predictions exhibit significant anisotropy due to the directional variations in the degrees of microcracking and healing.
- a series of simulations, including a parametric study, shows that the overall microcracking-healing response is strongly dependent on the curing time parameter of the self-healing agent, as well as the degree of microcracking at which healing is assumed to commence:
- the proposed model can simulate different types of self-healing scenarios and is able to replicate the behaviour of structural elements undergoing simultaneous microcracking and healing.

CRediT authorship contribution statement

Sina Sayadi: Writing – review & editing, Writing – original draft, Visualization, Validation, Methodology, Investigation, Conceptualization. **Iulia Mihai:** Writing – review & editing, Validation, Supervision, Conceptualization. **Anthony Jefferson:** Writing – review & editing, Validation, Supervision, Conceptualization.

Declaration of competing interest

The authors declare that they have no known competing financial interests or personal relationships that could have appeared to influence the work reported in this paper.

Acknowledgement

This project has received funding from the European Union's Horizon 2020 research and innovation programme under the Marie Skłodowska-Curie grant agreement No 860006. We acknowledge the support of the Supercomputing Wales project, which is part-funded by the European Regional Development Fund (ERDF) via Welsh Government.

Appendix A. . Weights and corresponding directions for spherical numerical integration

Point number i, direction $\mathbf{r}_{di}$ (also equals the position on a unit hemisphere) and integration weights w_{di}.

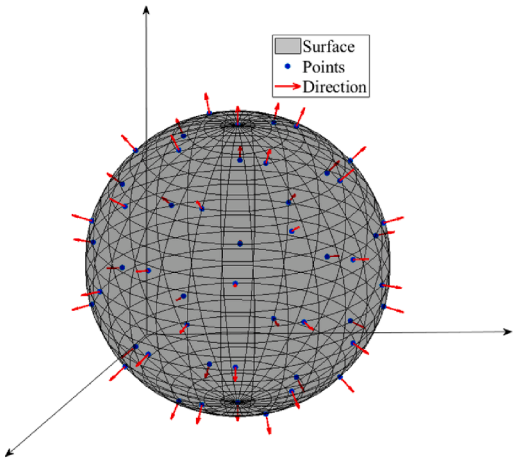

(a)

i	$\mathbf{r}_{di}$	w_{di}	i	$\mathbf{r}_{di}$	w_{di}
1	(1,0,0)	0.0254	16	$(\frac{\sqrt{3}}{3},\frac{\sqrt{3}}{3},\frac{-\sqrt{3}}{3})$	0.04219
2	(0,1,0)	0.0127	17	$(\frac{\sqrt{3}}{3},\frac{\sqrt{3}}{3},\frac{\sqrt{3}}{3})$	0.04219
3	(0,0,1)	0.0127	18	$(\frac{\sqrt{11}}{11},\frac{-\sqrt{11}}{11},\frac{-3\sqrt{11}}{11})$	0.04035
4	(0,-1,0)	0.0127	19	$(\frac{\sqrt{11}}{11},\frac{\sqrt{11}}{11},\frac{-3\sqrt{11}}{11})$	0.04035
5	(0,0,-1)	0.0127	20	$(\frac{\sqrt{11}}{11},\frac{-3\sqrt{11}}{11},\frac{-\sqrt{11}}{11})$	0.04035
6	$(\frac{\sqrt{2}}{2},\frac{-\sqrt{2}}{2},0)$	0.04515	21	$(\frac{\sqrt{11}}{11},\frac{-3\sqrt{11}}{11},\frac{\sqrt{11}}{11})$	0.04035
7	$(\frac{\sqrt{2}}{2},\frac{\sqrt{2}}{2},0)$	0.04515	22	$(\frac{\sqrt{11}}{11},\frac{-\sqrt{11}}{11},\frac{3\sqrt{11}}{11})$	0.04035
8	$(0,\frac{-\sqrt{2}}{2},\frac{-\sqrt{2}}{2})$	0.02257	23	$(\frac{\sqrt{11}}{11},\frac{\sqrt{11}}{11},\frac{3\sqrt{11}}{11})$	0.04035
9	$(0,\frac{-\sqrt{2}}{2},\frac{\sqrt{2}}{2})$	0.02257	24	$(\frac{3\sqrt{11}}{11},\frac{-\sqrt{11}}{11},\frac{-\sqrt{11}}{11})$	0.04035
10	$(0,\frac{\sqrt{2}}{2},\frac{-\sqrt{2}}{2})$	0.02257	25	$(\frac{3\sqrt{11}}{11},\frac{-\sqrt{11}}{11},\frac{\sqrt{11}}{11})$	0.04035
11	$(0,\frac{\sqrt{2}}{2},\frac{\sqrt{2}}{2})$	0.02257	26	$(\frac{3\sqrt{11}}{11},\frac{\sqrt{11}}{11},\frac{-\sqrt{11}}{11})$	0.04035
12	$(\frac{\sqrt{2}}{2},0,\frac{-\sqrt{2}}{2})$	0.04515	27	$(\frac{3\sqrt{11}}{11},\frac{\sqrt{11}}{11},\frac{\sqrt{11}}{11})$	0.04035
13	$(\frac{\sqrt{2}}{2},0,\frac{\sqrt{2}}{2})$	0.04515	28	$(\frac{\sqrt{11}}{11},\frac{3\sqrt{11}}{11},\frac{-\sqrt{11}}{11})$	0.04035
14	$(\frac{\sqrt{3}}{3},\frac{-\sqrt{3}}{3},\frac{-\sqrt{3}}{3})$	0.04219	29	$(\frac{\sqrt{11}}{11},\frac{3\sqrt{11}}{11},\frac{\sqrt{11}}{11})$	0.04035
15	$(\frac{\sqrt{3}}{3},\frac{-\sqrt{3}}{3},\frac{\sqrt{3}}{3})$	0.04219			

(b)

Fig. A1. Spherical integration directions, a) positions on a sphere, b) numerical integration directions and weights

Appendix B. . Thermodynamic consistency

The constitutive formulation should be consistent with the second law of thermodynamics. This may be satisfied, during healing, if the model ensures that no energy is created due to healing alone. The condition implies that the stress tensor in local and global coordinates before and after an increment of healing should be the same; thus, the corresponding eigenstrain for each healed set of microcracks is evaluated such that the overall global stress does not change due to healing alone. This condition may be expressed mathematically as follows, noting that here i and i-1 refer to states before and after a healing sub-step respectively:

$$\sigma_i = \mathbf{D}_{\text{sech}} : (\varepsilon - \varepsilon_{\text{ah}}) = \sigma_{i-1} \tag{B.1}$$

Re-arranging the above equation gives:

$$\varepsilon_{\text{ah}} = \varepsilon - \mathbf{D}_{\text{sech}}^{-1}\boldsymbol{\sigma}_{i-1} \tag{B.2}$$

ε_{ah} is given in equation (18). To allow for interaction effects between microcracking directions, a variable α has been added to the equation. The resulting equations in standard and discretised forms are given B.3 and B.4 respectively.

$$\boldsymbol{\varepsilon}_{\mathrm{Gh}} = \frac{1}{2\pi}\iint_S \boldsymbol{N}_{\varepsilon}\cdot\left[\frac{(1-\omega)}{h_v(1-\omega_h)}\boldsymbol{C}_{\mathrm{Lh}}\cdot\boldsymbol{D}_{\mathrm{L}} + \boldsymbol{I}^{2s}\right]^{-1} : \boldsymbol{\alpha} : \boldsymbol{\varepsilon}_{\mathrm{h}} \tag{B.3}$$

$$\boldsymbol{\varepsilon}_{\mathrm{Gh}} = \sum_{id=1}^{29} \mathbf{N}_{\varepsilon_{\mathrm{id}}} \bullet \left[\frac{(1-\omega_{id})}{h_{vid}(1-\omega_{h_{id}})}\mathbf{C}_{\mathrm{Lh}}\bullet\mathbf{D}_{\mathrm{L}} + \mathbf{I}^{2s}\right]^{-1} \alpha_{id}\varepsilon_{\mathrm{h\,id}} \tag{B.4}$$

The aim is to find α_{id} such that equation (B.1) is satisfied, with $\boldsymbol{\varepsilon}_{\mathrm{Gh}}$ in place of $\varepsilon_{\mathrm{ah}}$; however, this gives 6 equations with 87 unknowns as noted below. This equation is therefore an undetermined equation which has an infinite number of solutions. This may be resolved by applying the least squares constraint and assuming that $\mathbf{N}_{\varepsilon_{\mathrm{id}}} \bullet \mathbf{N}_{\varepsilon_{\mathrm{id}}} \bullet \left[\frac{(1-\omega_{id})}{h_{vid}(1-\omega_{h_{id}})}\mathbf{C}_{\mathrm{Lh}}\bullet\mathbf{D}_{\mathrm{L}} + \mathbf{I}^{2s}\right]^{-1}$ is a coefficient matrix for each direction considered (i.e. each spherical integration direction), as follows:

$$\sum_{id=1}^{29}\begin{bmatrix} C_{11}^{id} & C_{12}^{id} & C_{13}^{id} \\ C_{21}^{id} & C_{22}^{id} & C_{23}^{id} \\ C_{31}^{id} & C_{32}^{id} & C_{33}^{id} \\ C_{41}^{id} & C_{42}^{id} & C_{43}^{id} \\ C_{51}^{id} & C_{52}^{id} & C_{53}^{id} \\ C_{61}^{id} & C_{62}^{id} & C_{63}^{id} \end{bmatrix}\begin{bmatrix} \varepsilon_{h_1}^{id} \\ \varepsilon_{h_2}^{id} \\ \varepsilon_{h_3}^{id} \end{bmatrix}\alpha_{id} = \begin{bmatrix} \varepsilon_{Gh1} \\ \varepsilon_{Gh2} \\ \varepsilon_{Gh3} \\ \varepsilon_{Gh4} \\ \varepsilon_{Gh5} \\ \varepsilon_{Gh6} \end{bmatrix} \tag{B.5}$$

Expanding the above series leads to following 6 equations:

$$\begin{bmatrix} C_{11}^1\varepsilon_h^1 1 + C_{12}^1\varepsilon_h^1 2 + C_{13}^1\varepsilon_h^1 3 + C_{11}^2\varepsilon_h^2 1 + C_{12}^2\varepsilon_h^2 2 + C_{13}^2\varepsilon_h^2 3 & \cdots & C_{11}^{29}\varepsilon_h^{29} 1 + C_{12}^{29}\varepsilon_h^{29} 2 + C_{13}^{29}\varepsilon_h^{29} 3 \\ C_{21}^1\varepsilon_h^1 1 + C_{22}^1\varepsilon_h^1 2 + C_{23}^1\varepsilon_h^1 3 + C_{21}^2\varepsilon_h^2 1 + C_{22}^2\varepsilon_h^2 2 + C_{23}^2\varepsilon_h^2 3 & \cdots & C_{21}^{29}\varepsilon_h^{29} 1 + C_{22}^{29}\varepsilon_h^{29} 2 + C_{23}^{29}\varepsilon_h^{29} 3 \\ C_{31}^1\varepsilon_h^1 1 + C_{32}^1\varepsilon_h^1 2 + C_{33}^1\varepsilon_h^1 3 + C_{31}^2\varepsilon_h^2 1 + C_{32}^2\varepsilon_h^2 2 + C_{33}^2\varepsilon_h^2 3 & \cdots & C_{31}^{29}\varepsilon_h^{29} 1 + C_{32}^{29}\varepsilon_h^{29} 2 + C_{33}^{29}\varepsilon_h^{29} 3 \\ C_{41}^1\varepsilon_h^1 1 + C_{42}^1\varepsilon_h^1 2 + C_{33}^1\varepsilon_h^1 3 + C_{41}^2\varepsilon_h^2 1 + C_{42}^2\varepsilon_h^2 2 + C_{43}^2\varepsilon_h^2 3 & \cdots & C_{41}^{29}\varepsilon_h^{29} 1 + C_{42}^{29}\varepsilon_h^{29} 2 + C_{43}^{29}\varepsilon_h^{29} 3 \\ C_{51}^1\varepsilon_h^1 1 + C_{52}^1\varepsilon_h^1 2 + C_{33}^1\varepsilon_h^1 3 + C_{51}^2\varepsilon_h^2 1 + C_{52}^2\varepsilon_h^2 2 + C_{53}^2\varepsilon_h^2 3 & \cdots & C_{51}^{29}\varepsilon_h^{29} 1 + C_{52}^{29}\varepsilon_h^{29} 2 + C_{53}^{29}\varepsilon_h^{29} 3 \\ C_{61}^1\varepsilon_h^1 1 + C_{62}^1\varepsilon_h^1 2 + C_{33}^1\varepsilon_h^1 3 + C_{61}^2\varepsilon_h^2 1 + C_{62}^2\varepsilon_h^2 2 + C_{63}^2\varepsilon_h^2 3 & \cdots & C_{61}^{29}\varepsilon_h^{29} 1 + C_{62}^{29}\varepsilon_h^{29} 2 + C_{63}^{29}\varepsilon_h^{29} 3 \end{bmatrix} = \begin{bmatrix} \varepsilon_{Gh1} \\ \varepsilon_{Gh2} \\ \varepsilon_{Gh3} \\ \varepsilon_{Gh4} \\ \varepsilon_{Gh5} \\ \varepsilon_{Gh6} \end{bmatrix} \tag{B.6}$$

$$\begin{bmatrix} C_{11}^1 & C_{12}^1 & C_{13}^1 & C_{11}^2 & C_{12}^2 & C_{13}^2 & \cdots & C_{11}^{29} & C_{12}^{29} & C_{13}^{29} \\ C_{21}^1 & C_{22}^1 & C_{23}^1 & C_{21}^2 & C_{22}^2 & C_{23}^2 & \cdots & C_{21}^{29} & C_{22}^{29} & C_{23}^{29} \\ C_{31}^1 & C_{32}^1 & C_{33}^1 & C_{31}^2 & C_{32}^2 & C_{33}^2 & \cdots & C_{31}^{29} & C_{32}^{29} & C_{33}^{29} \\ C_{41}^1 & C_{42}^1 & C_{43}^1 & C_{41}^2 & C_{42}^2 & C_{43}^2 & \cdots & C_{41}^{29} & C_{42}^{29} & C_{43}^{29} \\ C_{51}^1 & C_{52}^1 & C_{53}^1 & C_{51}^2 & C_{52}^2 & C_{53}^2 & \cdots & C_{51}^{29} & C_{52}^{29} & C_{53}^{29} \\ C_{61}^1 & C_{62}^1 & C_{63}^1 & C_{61}^2 & C_{62}^2 & C_{63}^2 & \cdots & C_{61}^{29} & C_{62}^{29} & C_{63}^{29} \end{bmatrix}_{6\times 87} \begin{bmatrix} \alpha_1\varepsilon_{h_1}^1 \\ \alpha_1\varepsilon_{h_2}^1 \\ \alpha_1\varepsilon_{h_3}^1 \\ \alpha_2\varepsilon_{h_1}^2 \\ \alpha_2\varepsilon_{h_2}^2 \\ \alpha_2\varepsilon_{h_3}^2 \\ \vdots \\ \alpha_{29}\varepsilon_{h_1}^{29} \\ \alpha_{29}\varepsilon_{h_2}^{29} \\ \alpha_{29}\varepsilon_{h_3}^{29} \end{bmatrix}_{87\times 1} = \begin{bmatrix} \varepsilon_{Gh1} \\ \varepsilon_{Gh2} \\ \varepsilon_{Gh3} \\ \varepsilon_{Gh4} \\ \varepsilon_{Gh5} \\ \varepsilon_{Gh6} \end{bmatrix}_{6\times 1} \tag{B.7}$$

This is rewritten in matrix form as:

$$\varepsilon_{\mathrm{Gh}} = \mathbf{C}\alpha\varepsilon_h \tag{B.8}$$

Equation (B.8) is solved for the unknowns α, with $\varepsilon_{\mathrm{Gh}}$ in the right-hand-side being equal to $\varepsilon_{\mathrm{ah}}$ from equation (B.2).

Data availability

Data will be made available on request.

References

Abu Al-Rub, R.K., Darabi, M.K., 2012. A thermodynamic framework for constitutive modeling of time- and rate-dependent materials. Part I: Theory. *Int. J. Plast* 34. https://doi.org/10.1016/j.ijplas.2012.01.002.

Arnold, J.S., Adam, J.A., 1999. A simplified model of wound healing II: The critical size defect in two dimensions. *Mathematical and Computer Modelling* 30 (11–12). https://doi.org/10.1016/S0895-7177(99)00197-1.

Barbero, E.J., Greco, F., Lonetti, P., 2005. Continuum Damage-Healing Mechanics with application to self-healing composites. *Int. J. Damage Mech* 14 (1), 51–81.

Chen, Q., Li, W., Jiang, Z., 2022. Theoretical estimation of the elastic moduli of self-healing concrete relevant to the evolution of cracks closing due to crystallization- and precipitation-based mechanism. *Journal of Building Engineering* 58. https://doi.org/10.1016/j.jobe.2022.104995.

Cibelli, A., Pathirage, M., Cusatis, G., Ferrara, L., Di Luzio, G., 2022. A discrete numerical model for the effects of crack healing on the behaviour of ordinary plain concrete: Implementation, calibration, and validation. *Eng. Fract. Mech.* 263, 108266.

Darabi, M.K., Abu Al-Rub, R.K., Little, D.N., 2012. A continuum damage mechanics framework for modeling micro-damage healing. *Int. J. Solids Struct.* 49 (3–4). https://doi.org/10.1016/j.ijsolstr.2011.10.017.

Davies, R., Jefferson, A., 2017. Micromechanical modelling of self-healing cementitious materials. *Int. J. Solids Struct.* 113–114, 180–191.

Di Luzio, G., Ferrara, L., Krelani, V., 2018. Numerical modeling of mechanical regain due to self-healing in cement based composites. *Cem. Concr. Compos.* 86. https://doi.org/10.1016/j.cemconcomp.2017.11.006.

Dutta, S., Kishen, J.M.C., 2019. Micromechanical Damage Model for Plain Concrete Considering Propagation of Matrix Microcracks. *Phys. Mesomech.* 22 (2), 96–106.

Ferrara, L., Krelani, V., Carsana, M., 2014. A "fracture testing" based approach to assess crack healing of concrete with and without crystalline admixtures. *Constr. Build. Mater.* 68. https://doi.org/10.1016/j.conbuildmat.2014.07.008.

Freeman, B.L., Jefferson, A.D., 2022. A 3D coupled chemo-mechanical model for simulating transient damage-healing processes in self-healing cementitious materials. In *Computational Modelling of Concrete and Concrete Structures*. https://doi.org/10.1201/9781003316404-14.

Freeman, B.L., Jefferson, A., 2023. A 3D Coupled Finite-Element Model for Simulating Mechanical Regain in Self-Healing Cementitious Materials. *J. Eng. Mech.* 149 (7), 04023038.

Han, K., Ju, J.W., Zhang, H., Zhu, Y., Chang, T.-S., Wang, Z., 2021a. Mechanical response analysis of self-healing cementitious composites with microcapsules subjected to tensile loading based on a micromechanical damage-healing model. *Constr. Build. Mater.* 280. https://doi.org/10.1016/j.conbuildmat.2021.122251.

Han, K., Ju, J.W., Zhang, H., Zhu, Y., Chang, T.-S., Wang, Z., 2021b. Mechanical response analysis of self-healing cementitious composites with microcapsules subjected to tensile loading based on a micromechanical damage-healing model. *Constr. Build. Mater.* 280, 122251.

James, G., M., H. M., Tyson, R., Michele, B., Ayman, O., & Somayeh, A. (2014). Dicyclopentadiene and Sodium Silicate Microencapsulation for Self-Healing of Concrete. *Journal of Materials in Civil Engineering*, **26**(5), 886–896.

Jefferson, A., Bennett, T., 2007. Micro-mechanical damage and rough crack closure in cementitious composite materials. *Int. J. Numer. Anal. Meth. Geomech.* 31, 133–146.

Jefferson, A.D., Bennett, T., 2010. A model for cementitious composite materials based on micro-mechanical solutions and damage-contact theory. *Comput. Struct.* 88 (23), 1361–1366.

Jefferson, A.D., Freeman, B.L., 2022. A crack-opening-dependent numerical model for self-healing cementitious materials. *Int. J. Solids Struct.* 244–245, 111601.

Königsberger, M., Pichler, B., Hellmich, C., 2020. Multiscale poro-elasticity of densifying calcium-silicate hydrates in cement paste: An experimentally validated continuum micromechanics approach. *Int. J. Eng. Sci.* 147, 103196.

Lee, F.B., Anthony, J., 2023. A 3D Coupled Finite-Element Model for Simulating Mechanical Regain in Self-Healing Cementitious Materials. *J. Eng. Mech.* 149 (7), 04023038.

Mergheim, J., Steinmann, P., 2013. Phenomenological modelling of self-healing polymers based on integrated healing agents. *Comput. Mech.* 52 (3). https://doi.org/10.1007/s00466-013-0840-0.

Mihai, I.C., Jefferson, A.D., 2011. A material model for cementitious composite materials with an exterior point Eshelby microcrack initiation criterion. *Int. J. Solids Struct.* 48 (24), 3312–3325.

Monchiet, V., Gruescu, C., Cazacu, O., Kondo, D., 2012. A micromechanical approach of crack-induced damage in orthotropic media: Application to a brittle matrix composite. *Eng. Fract. Mech.* 83, 40–53.

Oucif, C., Mauludin, L.M., 2018. Continuum damage-healing and super healing mechanics in brittle materials: A state-of-the-art reviews. *Applied Sciences (switzerland)*. https://doi.org/10.3390/app8122350.

Pensée, V., Kondo, D., Dormieux, L., 2002. Micromechanical Analysis of Anisotropic Damage in Brittle Materials. *Journal of Engineering Mechanics-Asce - J ENG MECH-ASCE* 128. https://doi.org/10.1061/(ASCE)0733-9399(2002)128:8(889).

Pichler, B., Hellmich, C., A. Mang, H., & Aaaa, A. (2007). A combined fracture-micromechanics model for tensile strain-softening in brittle materials, based on propagation of interacting microcracks. *International Journal for Numerical and Analytical Methods in Geomechanics*, **31**(2), 111–132.

Pichler, B., Hellmich, C., 2011. Upscaling Quasi-Brittle Strength of Cement Paste and Mortar: A Multi-Scale Engineering Mechanics Model. *Cem. Concr. Res.* 41, 467–476.

Pichler, B., Hellmich, C., Eberhardsteiner, J., Chanvillard, G., 2013. Effect of gel–space ratio and microstructure on strength of hydrating cementitious materials: An engineering micromechanics approach. *Cem. Concr. Res.* 45, 55–68.

Ponnusami, S.A., Krishnasamy, J., Turteltaub, S., van der Zwaag, S., 2019. A micromechanical fracture analysis to investigate the effect of healing particles on the overall mechanical response of a self-healing particulate composite. *Fatigue Fract. Eng. Mater. Struct.* 42 (2). https://doi.org/10.1111/ffe.12929.

Sanz-Herrera, J.A., Aliko-Benitez, A., Fadrique-Contreras, A.M., 2019. Numerical investigation of the coupled mechanical behavior of self-healing materials under cyclic loading. *Int. J. Solids Struct.* 160, 232–246.

Selvarajoo, T., Davies, R., Freeman, B., Jefferson, A., 2020. Mechanical response of a vascular self-healing cementitious material system under varying loading conditions. *Constr. Build. Mater.* 254, 119245. https://doi.org/10.1016/j.conbuildmat.2020.119245.

Shields, Y., De Belie, N., Jefferson, A., Van Tittelboom, K., 2021. A review of vascular networks for self-healing applications. *Smart Mater. Struct.* 30 (6), 063001.

Simo, J.C., Hughes, T.J.R., 1998. Computational Inelasticity. Springer.

Stroud, A.H., 1973. Approximate Calculation of Multiple Integrals. Mathematics of Computation 27 (122). https://doi.org/10.2307/2005635.

Subramanian, H., Mulay, S.S., 2022. On the constitutive modelling of elasto-plastic self-healing materials. *Int. J. Solids Struct.* 234–235. https://doi.org/10.1016/j.ijsolstr.2021.111289.

Van Tittelboom, K., De Belie, N., 2013. Self-healing in cementitious materials-a review. *Materials* 6 (6). https://doi.org/10.3390/ma6062182.

van Vermolen, F.J., Baaren, E., Adam, J.A., 2006. A simplified model for growth factor induced healing of wounds. *Math. Comput. Model.* 44 (9–10). https://doi.org/10.1016/j.mcm.2006.02.017.

Voyiadjis, G.Z., Shojaei, A., Li, G., 2011. A thermodynamic consistent damage and healing model for self healing materials. *Int. J. Plast* 27 (7). https://doi.org/10.1016/j.ijplas.2010.11.002.

Zhou, S., Zhu, H., Yan, Z., Ju, J.W., Zhang, L., 2016. A micromechanical study of the breakage mechanism of microcapsules in concrete using PFC2D. *Constr. Build. Mater.* 115, 452–463.

Zhou, S., Zhu, H., Ju, J.W., Yan, Z., Chen, Q., 2017. Modeling microcapsule-enabled self-healing cementitious composite materials using discrete element method. *Int. J. Damage Mech* 26 (2). https://doi.org/10.1177/1056789516688835.

Zhu, C., Arson, C., 2014. A thermo-mechanical damage model for rock stiffness during anisotropic crack opening and closure. *Acta Geotech.* 9 (5), 847–867.

Zhu, H., Zhou, S., Yan, Z., Ju, J.W., Chen, Q., 2015. A two-dimensional micromechanical damage-healing model on microcrack-induced damage for microcapsule-enabled self-healing cementitious composites under tensile loading. *Int. J. Damage Mech* 24 (1), 95–115.

Zhu, H., Zhou, S., Yan, Z., Ju, J.W., Chen, Q., 2016. A two-dimensional micromechanical damage–healing model on microcrack-induced damage for microcapsule-enabled self-healing cementitious composites under compressive loading. *Int. J. Damage Mech* 25 (5), 727–749.